THESIS
R-56/w
1986
c.2

WOLFRAMITE:

AN INFRARED EXAMINATION OF TRANSPARENCY CONTROLS AND FLUID INCLUSIONS

N.M.I.M.T.
LIBRARY
SOCORRO, N.M.

by

Sylveen E. Robinson-Cook

Geophysical Information Center

Submitted in Partial Fulfillment
of the Requirements for the Degree of
Master of Science in Geology

New Mexico Institute of Mining and Technology

Socorro, New Mexico

April, 1986

AC6 7 1986

14061397

ABSTRACT

This study is an attempt to validate the use of the infrared microscope in ore deposits research via a two pronged approach. In the first section the controls of infrared transparency in the ore mineral wolframite are examined and in the second part the uses of the infrared microscope in fluid inclusion analysis are examined.

Infrared light (0.8-1.2 microns) has been used to determine the infrared transparency of the mineral wolframite [$FeMn(WO_4)$]. In the initial examination of 14 wolframite samples from locations around the world it was found that the samples had variable infrared transparency with 5 samples completely opaque and 9 samples which were transparent to a greater or lesser degree. The control of infrared transparency in wolframite was hypothesized to be geochemical in nature and a comprehensive study of the geochemistry of the 14 wolframite samples was initiated. XRF, NAA, and microprobe analysis provided quantitative information on the wolframite compositions and XRD analysis defined wolframite mineralogy. In those wolframites which were transparent, a rough correlation was noted between transition element (Cr, Co, Ni, and Zn) concentration and degree of infrared transparency. This trend is analogous to the dark coloration such elements cause in visible light in

minerals such as cassiterite (SnO_2). However, these results proved inconclusive for determining the geochemical control of wolframite infrared opacity. No element or group of elements analysed for in this study could be conclusively proven to contribute to infrared opacity.

In the second section of this study, transparent wolframite samples were examined for fluid inclusions and their data compared to that obtained from cogenetic quartz in an attempt to address the validity of the common assumption that P-T-X conditions of ore formation can be accurately determined from gangue phases.

Of the four wolframite deposits examined, two provided wolframite data in excellent agreement to data obtained from quartz. The Black Pine Mine, Montana huebnerite (Mn-rich wolframite) had temperatures of homogenization ranging from 210 to 280°C with salinities of 5.1 to 8.1 equivalent weight percent NaCl which is a similar range as fluid inclusion data from quartz at this deposit.

The San Cristobal, Peru wolframite samples provided temperatures of homogenization ranging from 195 to 330°C and salinities of 1.6 to 6.6 equivalent weight percent NaCl. This is in excellent agreement with fluid inclusion data from Campbell et al. (1984) who report temperatures of homogenization for quartz from this deposit ranging from 150 to 350°C and salinities of 2.7 to 6.3 equivalent weight

percent NaCl.

The Panasqueira, Portugal wolframite samples became infrared opaque before temperatures of homogenization could be determined but inclusion types noted in wolframite are identical to those reported in wolframite-stage quartz by Kelly and Rye (1979). Salinities obtained from wolframite range slightly higher (8-13 equivalent weight percent NaCl) than those for quartz (5-10 equivalent weight percent NaCl) but are considered to be compatible.

The fourth wolframite deposit, Victorio Mountains, New Mexico, had an extreme discrepancy in fluid inclusion data obtained from the quartz versus that obtained from wolframite. Temperatures of homogenization from quartz (141-320^{o}C) were approximately 100^{o}C lower than temperatures from wolframite (280-380^{o}C) and salinities for quartz were in general lower than wolframite salinities. The quartz inclusions were extremely CO_2-rich having a liquid CO_2 phase at room temperature with evidence of CO_2 effervescence throughout quartz deposition. Only one CO_2-rich inclusion was noted in wolframite.

It can be concluded that P-T-X data collected from ore as well as gangue phases is essential in understanding the depositional history of an ore deposit. The infrared microscope has proven to be an important tool in the collection of fluid inclusion data from an opaque ore

mineral.

ACKNOWLEDGMENTS

The primary responsibility for the inspiration and instigation of this research must lie on the sholders of Dr. Andrew Campbell. I wish to thank him for providing me with such an interesting research project and for never waning in his enthusiasm for this research. My thanks to Dr. Jacques Renault for the long hours of discussion and helpful guidance he provided throughout the course of this study. Thanks also to Dr. Fred Kuellmer for his direction and guidance.

This thesis was parially funded through grant 9C-EF-04-9 from the State Mining and Mineral Resources Research Institute and through a Grant-in-Aid from the New Mexico Geological Society.

I wish to thank all the people who donated wolframite samples for this study; Dr. Kevin Shelton from the University of Missouri-Columbia, Mr. Bob North and Dr. Bob Weber of the New Mexico Bureau of Mines and Mineral Resources, Dr. William Kelly of the University of Michigan-Ann Arbor, Mr. Carl Dotson of United Minerals of Socorro, and Mr. Forrest Cureton of Cureton Mineral Company of Tuscon, AZ.

A special thanks to Dr. Phillip Kyle for providing the Neutron Activation Analysis and the Los Alamos National Laboratory for use of their microprobe laboratory.

No research is ever completed without the exchange of ideas, hopes, disappointments and worries with one's peers. I can only say thank you to my friends and fellow graduate students for the wealth of information obtained from my interactions with you.

Finally and forever, my love and gratitude to my husband, Kevin, for putting up with my ups and downs for the last few years.

TABLE OF CONTENTS

LIST OF FIGURES

LIST OF TABLES

INTRODUCTION

STATEMENT OF PROBLEM

Until recently, microscopic studies of ore deposits have been predominantly restricted to reflected light ore petrography and transmitted light studies on transparent gangue minerals. Campbell et al. (1984) discuss a new tool for ore deposit studies, the infrared microscope. This microscope transmits near-infrared light (0.8-1.2 microns) through ore minerals normally opaque allowing for optical observations in transmitted light. Campbell et al. (1984) present a brief examination of several opaque ore minerals which they found were transparent in the infrared. Continuing along the same lines as that preliminary study, the present study was developed in an attempt to establish the validity of the infrared microscope in ore deposit studies by doing a detailed examination of its use in fluid inclusion determinations. However, in this study's preliminary examination of some opaque ore minerals using the infrared microscope, it was found that several of these minerals exhibit variable transparency in infrared light. Understanding the factors controlling infrared transparency in these minerals became the first objective of this research. In this manner a two pronged approach was developed. Section I will deal with the research used to

attempt to identify the factor(s) controlling infrared transparency in a single mineral. Section II will detail the application of the infrared microscope in fluid inclusion research.

SECTION I

Introduction

In the initial stage of this study many minerals were examined to determine infrared transparency. Transparency determinations were made on slides of doubly polished thick sections. Table 1 lists the minerals examined in the initial stage and their localities and whether they were transparent in the infrared spectrum. All of these minerals are opaque in visible light.

It must be noted that many of these minerals show a wide range of compositions as they are members of a solid solution series. The transparency noted may well be linked to composition but, on the samples examined, no compositional information was available. The formulas listed are the ideal stoicheometric values. Transparency is hypothesized to be governed by geochemistry. To accomplish both goals of this study, a mineral had to be chosen which shows a variable infrared transparency and was adequate for fluid inclusion study.

Wolframite, was chosen for an extensive study of the controls on infrared transparency and a detailed study of fluid inclusions. The wolframite mineral series [$(Fe,Mn)WO_4$] shows extreme variability in infrared transparency between samples which is ideal for geochemical testing and correlations. Wolframite samples from 13

deposits around the world were collected for use in this study (Table 2).

LIST OF MINERALS EXAMINED FOR INFRARED TRANSPARENCY

MINERAL	LOCATION	FORMULA	TRANSPARENT
Argentite	Mexico	Ag_2S	NO
Bornite	New Mexico	Cu_5FeS_4	NO
Bournonite		$PbCuSbS_3$	SLIGHTLY
Chalcocite	New Mexico	Cu_2S	NO
Chalcopyrite	New Mexico	$CuFeS_2$	NO
Chromite	Idaho	$FeCr_2O_4$	NO
Covellite	Butte,Mt	CuS	NO
Enargite		Cu_3AsS_4	YES
Freibergite	Lovelock,Nv	$Cu_{12}(Ag)Sb_4S_{13}$	YES
Molybdenite	Questa, NM	MoS_2	VARIABLY
Pyragyrite	Hermosa, NM	Ag_3SbS_2	SLIGHTLY
Pyrite	New Mexico	FeS_2	NO
Siderite		$FeCO_3$	SLIGHTLY
Stibnite	New Mexico	Sb_2S_3	SLIGHTLY
Tennantite		$Cu_{12}As_4S_{13}$	YES
Tetrahedrite	New Mexico	$Cu_{12}Sb_4S_{13}$	YES
Wolframite	San Cristobal, Peru	$(Fe,Mn)WO_4$	VARIABLY

VARIABLY: transparency changes within and between sections
SLIGHTLY: transparency not enough for optical observations

TABLE 2

WOLFRAMITE SAMPLES

ALPHABETICALLY LISTED ACCORDING TO LOCATION

SAMPLE IDENTITY ABBREVIATIONS/ SAMPLE LOCATION	SAMPLE #	TRANSPARENCY*
(TT) Tiptop, Arizona	--	0
(BN) Bolsa Negra Bolivia	9500	4.5
(SP) Sao Paulo Brazil	8028	0
(CE) Cornwall England	812.6	4.0
(HK) Needle Hill Mine Hong Kong	79.79	0
(JP) Kafoshima Japan	--	0
(MO) Silvermines, Missouri	2013	4.5
(BP) Black Pine, Montana	--	7.3
(NV) Nevada	--	4.2
(WO) White Oaks, NM	8658	0
(VM) Victorio Mts. NM	846	6.5
(SC) San Cristobal, Peru	SC-9	6.5
(PP) Panasqueira Portugal	G-37	7.1
(SD) Lawrence Co. So Dak.	--	4.3

*Transparency measured on scale of 0-12 But, measurements made with no sample in the path of the light were 8. This must be considered 100% transmission.

HYPOTHESIS

Three factors are suggested which may explain variations in the transmission of infrared light in wolframite.

1- Major element composition
In the visible spectrum the manganese rich end member of the wolframite series, huebnerite ($MnWO_4$) is transparent. As iron substitutes into huebnerite, visible transparency rapidly decreases. This would seem to indicate that the iron concentration may control transparency in the infrared spectrum also.

2- Minor element composition
Wolframite, like most minerals, contains small amounts of non-stoichiometric elements. The concentration and identity of these trace contaminents varies from sample to sample. An increase of one element or a combination of elements may change infrared transmission by three processes;
   a) distorting the crystal lattice (Goncharov et al. 1971), due to the substituting element's ionic size, valence, electronegativity, etc.
   b) due to preferential absorption of near infrared radiation by the substituting element or
   c) due to the presence of lattice defects caused by radioactive decay of a contaminent (Swart and Moore, 1982).

3- Crystallographic control
The infrared transmission along the optical axes may vary considerably. This variation might render one orientation 'infrared opaque'.

APPROACH

In order to determine the correlation between transparency and geochemistry, the wolframite samples were examined using one or more of the following analytical techniques:

1-Each section of wolframite was examined for infrared transparency using polished sections as well as cleavage chips.
2-Polished thick sections were made perpendicular to the c crystallographic axis of wolframite crystals and examined for variations in infrared transparency.
3-X-ray fluorescence spectrometry (XRF) was used to determine major and trace element composition for each sample.
4-X-ray diffraction (XRD) was used to determine the presence of separate mineral phases within each sample of wolframite.
5-Microprobe was used to determine compositional variations in major elements between highly transparent areas and opaque areas.
6-Neutron Activation (NAA) was used to determine the concentration of 22 trace elements.

PREVIOUS STUDIES

Saldanha (1947), Ganeev et al. (1960), and Guillen et al. (1985) geochemically analyzed wolframites and have reported various trace element contaminents within them. The most common trace elements found in wolframite are Nb, Ta, Mg, Sc, Y, U and Sb. Guillen et al. (1985) also reported the presence of Fe^{+3}. As wolframite is opaque in visible light, none of these studies related the chemical analysis to optical transparency.

Cassiterite exhibits the same transparency variation in the visible spectrum that wolframite exhibits in the near infrared spectrum. A similar process may control transparency in both minerals. Many researchers have attempted to establish a relationship between chemical composition and color banding in cassiterite. Pecora et

al. (1950) found an increase of Nb and Ta in the darker bands of cassiterite. Noll (1949) and Goncharov et al. (1971) found that increasing contents of Fe, W, Ba, Sc, Be and Mn cause anisotropic lattice deformation producing brown colorations in cassiterite. Berzina and Dolomanova (1967) and Swart and Moore (1982) reported an increase in U in the darker bands of cassiterite. Cuff (1979) found that Mn, Ti, Ta, Nb, Ni, Co and Cu increased in varying amounts with the highest concentrations found in brown to black cassiterite.

SAMPLE SELECTION

Wolframite samples used in this study were collected from various individuals and museums. With the exception of four deposits, Panasqueira, San Cristobal, Victorio Mountains and White Oaks, only one hand sample was available from each deposit. Not all samples were suitable for all aspects of this study. Samples used for the determination of infrared transparency had to have fairly large crystals. Microcrystalline samples were unsuitable as they are opaque due to the high internal reflection of light at crystal boundaries rather than a chemical constituent. The presence of large cleavage faces was also important as chips of variable thickness could be easily made. Thickness is a major control of transparency in some wolframites.

was done on every sample and care was taken to use unaltered wolframite. Some samples were universally fractured and highly altered which was noted. The major consideration in sampling was the occurrence of a transparent gangue phase with wolframite. In most of the samples studied, quartz was the primary coexisting gangue. However, not every sample contained a gangue phase.

ANALYTICAL TECHNIQUES

Physics of Infrared Absorption

The absorption of the wavelengths of light used in this study occurs within a mineral at the electron scale. The absorption of specific wavelengths causes the mineral to appear colored or exhibit pleochroism. These effects are most often due to the presence of transition metal or lanthanide elements in the crystal structure as trace or major chemical constituents. These elements produce coloring/pleochroism effects by several processes, the most common being electron transfer processes which affect wavelengths from the ultraviolet to the infrared (Burns 1971). Electron transfers may be induced by several means.

a). Internal electron transitions within transition metal and lanthanide elements. These transitions occur by the excitation of electrons between d (transition) and f (lanthanide) orbitals where the energy of separation is in the range of 2.5 to 1.4 microns. The wavelengths absorbed determine the color produced.
b). Inter-element electron transitions or charge transfers. This process is caused by ultraviolet radiation which produces photo-chemical oxidation-reduction causing electrons to migrate between ions within a crystal structure.
c). Electron transitions can be induced by crystal structure imperfections. Here lattice defects absorb light and become color centers. Lattice defects can be due to radioactive decay as is observed in pleochroic halos around biotites and in irradiated fluorite or halite.
d). Band-gap transitions. When the energy of the absorbed wavelength is equal to the energy difference between the conduction band and the valence band, a band gap transition occurs. This produces an absorption edge. This process is equivalent to the absorption processes in x-ray spectrometry.

INFRARED OPTICS

In this study, the Research Devices Model F infrared microscope (fig. 1) was used to study internal features of wolframite and determine transparency. The Model F infrared microscope is a polarizing microscope equipped with a high intensity light source (100 watts) and an infrared converter. Light is filtered to the accepted infrared wavelengths (8000 to 12000A) as it passes through a visible light filter. The sample is illuminated by this infrared light using either transmitted or reflected modes. The infrared light enters the main barrel containing an image converter tube.

The converter tube works by projecting the image from the objective onto the front of a half-transparent cathode in the imaging tube. The electrons pulled out of the cathode are focused onto the fluorescent exit screen by a series of electronic lenses. This produces a visible 'real' image at the exit lense which is further magnified and telescoped to the binocular eyepieces. The resolution is limited by the crystallinity of the fluorescent exit screen.

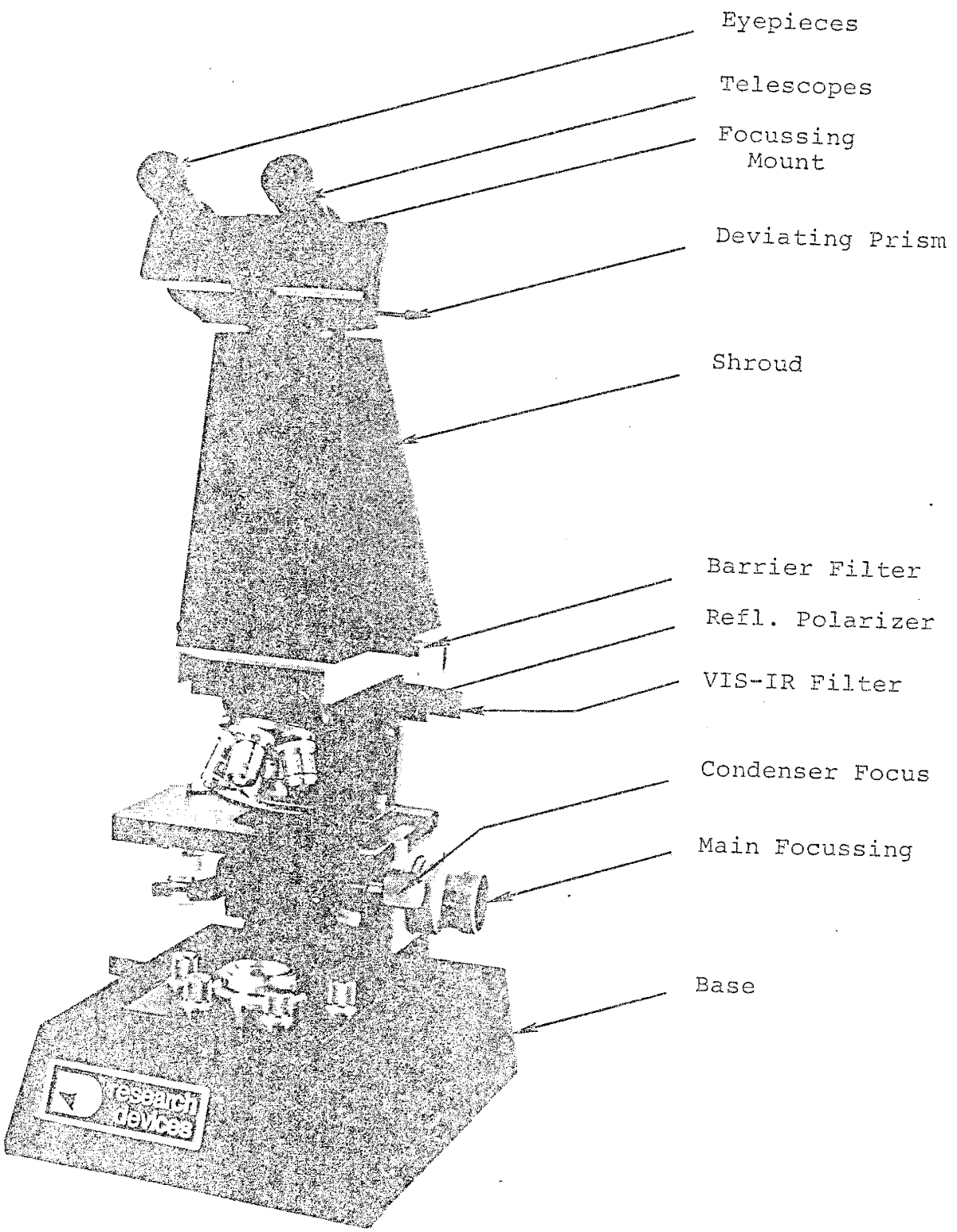

Figure 1. Model F Infrared Microscope

(Right Side)

MINERALOGY OF WOLFRAMITE

Wolframite is a monoclinic tungstate mineral of iron and manganese $(Fe,Mn)WO_4$. The series ranges from the iron end-member FERBERITE ($FeWO_4$) to the manganese end-member HUEBNERITE ($MnWO_4$). The accepted definition for the chemical content for these minerals is:

FERBERITE	100-80 mole % FeWO4
WOLFRAMITE	80-20 mole % FeWO4
HUEBNERITE	20-0 mole % FeWO4

Unless otherwise stated, the term 'wolframite' will be used in this text to refer to all members of the solid solution series.

The stoichiometric concentrations for wolframite are; WO_3 (76.3%), FeO (23.7%) for ferberite and WO_3 (76.6%) MnO (23.4%) for huebnerite. Quartz and base metal sulfides are the principal minerals found in association with wolframite. Other, less common phases include cassiterite (SnO_2), scheelite ($CaWO_4$), hematite (Fe_2O_3) and fluorite (CaF_2).

In the wolframite structure (figure 2) the oxygen ions form a slightly distorted hexagonal close-packed structure (Guillen and Regnard, 1985). One half of the octahedral sites are filled. Of these, 1/2 are occupied by Fe+2/Mn+2 ions and 1/2 are occupied by W+4 ions. The structure is further ordered by the layering of Fe+2/Mn+2 octahedrons alternating with layers of W+4 octahedrons along the (100)

direction. Chains of Fe+2/Mn+2 octahedrons sharing edges zig-zag along the c-axis. Unit cell parameters have been shown to vary linearly with the x value (Sasaki, 1959). Thus the variation of the a-parameter with x can be used to calibrate the Fe/Mn solid solution.

The geochemical analysis of wolframite was designed to test for specific elements. These trace elements were chosen for several reasons. Ni, Co, Zn and Mg were selected for their similarity to Fe+2/Mn+2 in valences and ionic radii. Mo was selected due to its similarity to W+4 in valence and ionic radii and due to the limited solid solution of Mo and W in the scheelite/powellite series. Pb is a common element associated with tungsten both as separate tungsten phases (powellite, stolzite) and in limited solid solution with Mn (Palache et al. 1951). Sc has been reported in many wolframite analyses. Ganeev and Sechina (1960) proposed a coupled substitution of Sc and Y into the wolframite structure by:

$$3Fe^{+2} + 3Mn^{+2} = 2Sc^{+3} + 2Y^{+3}$$

The analytical techniques for XRF, XRD, NAA and microprobe are listed in Appendix I.

Figure 2: A schematic drawing of the wolframite structure. (Modified from Ulku, 1967)

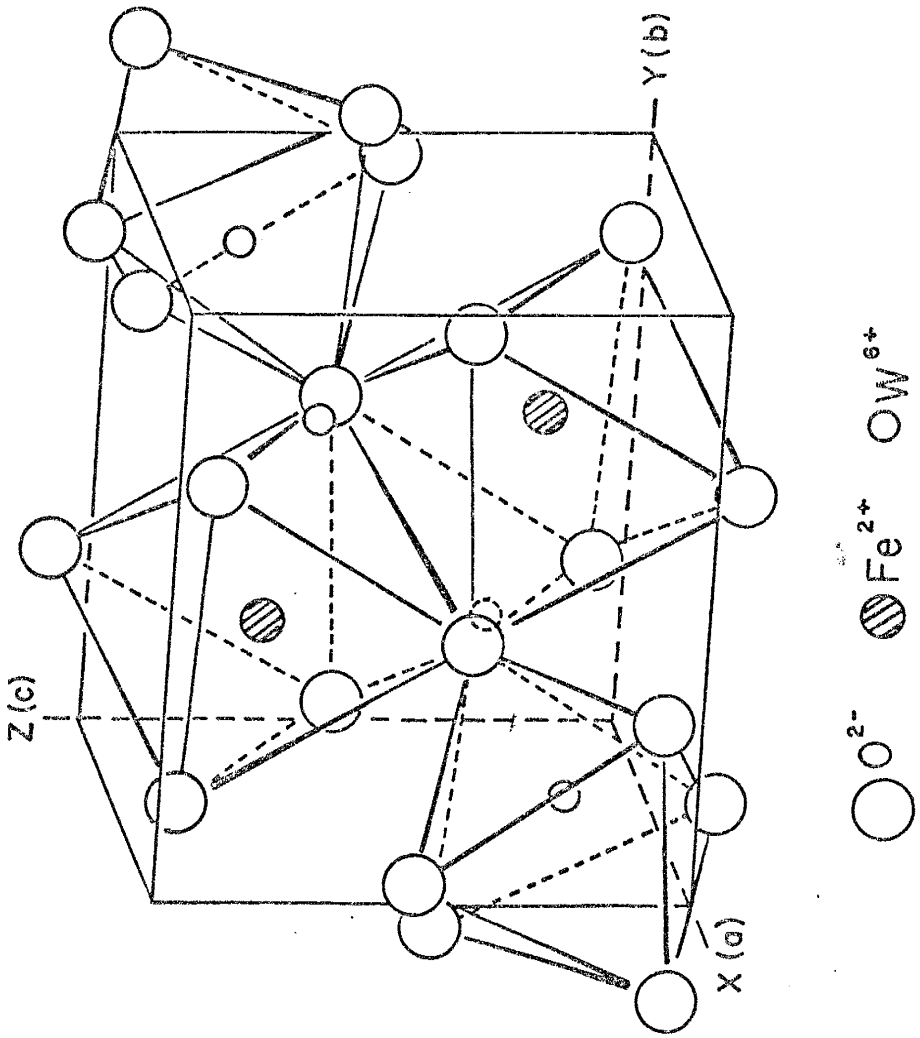
Y (b)
Z (c)
X (a)
O^{2-}
Fe^{2+}
W^{6+}

ANALYTICAL RESULTS

INFRARED OPTICAL OBSERVATIONS

Six of the wolframite samples examined were completely opaque in the infrared, even with very thin cleavage chips (.09 inch). One deposit, Victorio Mts. NM, yielded both opaque and transparent samples. Two others, (Panasqueira and San Cristobal) were always transparent but the transparency of the San Cristobal wolframite was very dependent upon thickness. The Black Pine deposit contained huebnerite which was transparent in both visible and infrared light. The other five wolframite samples were somewhat transparent yet the transparency was not enough to facilitate optical observations. Transparency was measured on cleavage chips with a photo-electric cell attached to the infrared microscope. Thickness was standardized to 0.09 inch by using cleavage chips which were broken to 0.09 inches thick. If it was impossible to create a chip of exactly 0.09 inches, transparency measurements were made on a range of thickness and a transparency curve was created with the value at 0.09 inches interpolated from this curve.

The four wolframites which were transparent were examined and optical observations were noted for each.

Panasqueira, Portugal (PP)

Polished sections of Panasqueira wolframite proved to be extremely transparent in the infrared. Internal features which were noted included areas of intense banding, areas of dense inclusions and areas which were void of any observable features. It was noted that sections which were cut perpendicular to the cleavage plane exhibited dense populations of fluid inclusions. Banding when noted seemed to follow crystal orientations providing strong evidence for their origin being due to growth planes.

San Cristobal, Peru (SC)

San Cristobal section transparency was extremely dependant upon thickness of the sections. In several sections banding was so strong it occluded optical observations. Banding was evident in every sample and in most sections was the dominant feature. Fluid inclusions were present in limited amounts. The majority of inclusions seemed to have been preferentially trapped along crystal growth planes parallel to the c-axis. This causes dense populations of fluid inclusions along the cleavage plane (010).

Victorio Mountains, New Mexico (VM)

The Victorio Mountains wolframite samples proved to be of variable transparency within each section. The opaque areas do not seem to be dependant upon any crystallographic control as they are universal despite the sample orientation. The opaque/transparent boundaries are often diffuse and do not correspond to crystallographic orientations. They are not believed to be growth banding. The opaque areas appear to more closely resemble a later generation of opaque wolframite occupying cracks and fractures in a transparent wolframite. This fracture filling stage does not cross into the surrounding quartz so it is possible that there was not any significant time period between development of the two types of wolframite. The wolframite is also extensively veined and altered by iron-oxides. Banding is rarely noted. In areas where it occurs, the banding is correlatable between adjacent transparent patches providing further evidence for the later crosscutting relationship of the opaque wolframite. Similar relationships have been found in cassiterite at the Herberton Queensland, Australia deposit by Georgees (1974). Quartz and wolframite exhibit intergrowth textures such as euhedral wolframite crystals enclosed by quartz, small quartz crystals encased by wolframite, and solid inclusions of wolframite in quartz.

Black Pine, Montana (BP)

As this is a huebnerite sample, it is transparent in both visible and infrared light. Banding is noted in visible light. Some bands grade into opaque areas. These same areas are transparent when observed in the infrared. Fluid inclusions are noted in every section. Wolframite and quartz are intimately intergrown. Quartz crystals terminate against huebnerite crystals, solid inclusions of huebnerite are common in quartz crystals and many other signs indicate cogenetic growth of both minerals.

MINERALOGY

X-ray Diffraction

Fourteen wolframite samples were analysed on a Rigaku x-ray diffractometer equipped with a monochromator using Ni filtered Cu-K radiation and a scintillation counter. As the X-ray diffraction mounts were the same as those used for x-ray fluorescence spectrometry, no internal standard could be used. Thus, in order to achieve as accurate a measurement of the wolframite's d-spacings as possible, a step scan was used with 0.020° 2θ steps counted for 0.2 seconds each. The scans were made between $2\theta=13^{\circ}$ and 70° corresponding to values of d between 6.657 and 1.344A. Count data were analysed by the Rigaku Peak Analysis computer program where 2θ values, d-spacing values, intensities and 1/2 peak height width values were calculated. Table 3 contains d-spacing values greater than 2.054A for all the analysed wolframites. Ten duplicate determinations using CERAC $FeWO_4$ and $MnWO_4$ standards verified that the diffraction angles could be determined to +/- 0.05 degrees 2θ.

Table 3: d-spacings for 13 wolframite samples and 2 wolframite standards. Listed in order of mole % $MnWO_4$ as determined from geochemical analysis.

REI	MNWO4	BP	MO	BV	MO	VM	SO	NK	SP	CE	JP	TT	BN	PP	FEWO4	REI
(010)	5.779	5.779	5.764	5.764	5.749	5.771	5.757	5.757	5.757	5.742	5.734	5.727	5.727	5.719	5.719	(010)
(100)		4.844	4.834	4.828	4.813	4.828	4.797		4.782	4.767	4.762			4.752		(100)
(011)	3.776	3.779	3.779	3.776		3.776	3.77		3.776	3.764	3.761	3.757	3.754		3.751	(011)
(110)	3.702	3.708	3.705	3.699	3.689	3.696	3.681	3.678	3.675	3.666	3.659	3.657	3.654	3.654	3.648	(110)
(111)	2.998		2.998	2.994	2.992	2.988	2.974	2.978							2.94	(111)
(111)	2.955	2.957	2.953	2.953		2.953	2.949		2.951	2.947	2.946	2.944	2.944	2.944	2.939	(111)
(020)	2.881	2.884	2.881	2.879	2.872	2.877	2.869	2.869	2.869	2.864	2.863	2.859	2.857	2.857	2.857	(020)
(002)	2.499	2.493		2.495	2.492	2.494	2.487		2.491	2.485	2.483		2.479	2.478		(002)
(120)	2.474		2.476		2.473	2.47	2.462				2.453		2.449		2.389	(120)
(200)	2.416		2.414	2.411			2.394	2.384	2.387	2.379	2.379	2.376	2.374		2.368	(200)
(102)	2.238				2.226		2.223	2.222		2.199				2.197	2.198	(102)
(121)	2.209		2.209			2.205	2.203	2.202	2.203							(121)
(112)	2.083					2.077			2.074							(112)
(112)	2.056					2.056		2.057	2.059		2.054	2.056				(112)
MOLE % MNWO4		99.7	99.5	88.6	73.8	69.9	48.4	44.8	42.9	32.6	27.6	17.1	15.5	14.8		

XRD data provided a variety of information. 1) It was used to determine the purity of the wolframite samples. 2) The d-spacing data was used to determine the amount of unit cell size variation among wolframite samples. 3) The peak width at half height for (100) was used in an attempt to determine the degree of crystal perfection of each sample.

1) Wolframite purity

Each sample's chart was analysed for the evidence of any separate mineral phases present within the wolframite sample. Positive evidence for a second or third phase was determined by the presence of three or more peaks for that mineral, one of which was required to be it's most intense peak (Cullity, 1956). The additional minerals identified within each sample are listed in Table 4. No quantitative analysis of the concentration of these minerals was done with XRD as a weight percent value was determined through XRF.

TABLE 4

X-RAY DIFFRACTION MINERAL IDENTIFICATION

SAMPLE	SEPARATE MINERAL PHASES PRESENT AS DETERMINED FROM XRD PATTERNS
(TT) Tiptop, AZ	quartz
(BN) Bolivia, Bolsa Negra	scheelite
(SP) Brazil	quartz
(CE) Cornwall	quartz
(HK) Hong Kong	scheelite
(JP) Japan	ZnWO4
(MO) Silvermines, MO	stolzite
(BP) Black Pine, MT	no separate phases present
(NV) Nevada	no separate phases present
(WO) White Oaks, NM	no separate phases present
(VM) Victorio Mts. NM	scheelite
(PP) Panasqueira, Port.	no separate phases present
(SD) South Dakota	quartz

2) Unit cell size variations

In any solid solution series, substitution of one cation for another will cause a slight change in the unit cell volume. This change is often considered to be linearly related to the amount of substitution and is called Vegard's Law. Several studies have used the presumed linear variation in wolframite's d-spacings to determine the Fe/Mn content [Sasaki (1959), Berman and Campbell (1957), Baumann and Starke (1964), and Sleight (1972)]. Sasaki (1959) reports that wolframite's cell dimensions vary linearly with composition. Hsu (1976) analysed synthetic wolframites for variations in d-values with Fe/Mn content. He reports a linear variation in wolframite's $d_{(200)}$ value with increasing mole % $MnWO_4$.

The validity of Vegard's law with respect to wolframite was tested by establishing a straight line between the two experimentally determined end members a CERAC $MnWO_4$ standard, and a CERAC $FeWO_4$ standard.

The CERAC standards were analysed using the same conditions as the wolframite samples. Wolframite unit cell dimensions were estimated from the d-spacings of the second order basal reflections of (002), (020), and (200). No first order peaks were used due to the greater error associated with these reflections. As a result, only 7 of the 13 wolframite samples can be included on this plot.

The accuracy of the $FeWO_4$ compositions were calculated using mole percents of WO_3, FeO, and MnO determined from geochemical analysis. The WO_3 mole % was assumed to be wholly contained by the wolframite phase. The MnO mole % was added to the WO_3 mole % with any excess WO_3 then added to the FeO mole %. This calculation was then repeated starting with the FeO mole % and ending with the MnO mole %. Variations in the compositions determined are expressed as horizontal bars.

Figure 3 plots the unit cell volume against mole % $FeWO_4$. The plot shows a close correlation of four points (NV, HK, SP, and JP) with the calibration curve. For three samples (SD, CE and BN) the correspondence is less good. Intermediate compositions of natural wolframites reported on JCPDS cards 21-436, 27-256, and 11-591 also fall off the straight line in a similar manner as the results reported here.

This deviation is considered significant in that all previous studies of natural wolframites have assumed the linear trend of wolframite data on such a plot even though it has only been tested using synthetic samples. The greatest deviation (SD) is equivalent to the effect of approximately 5 mole % less $FeWO_4$ as is shown by a horizontal tie line from this point to the curve.

FIGURE 3: A plot of the unit cell volume for 2 standard, 5 natural wolframites using data from their JCPDS cards and 7 natural wolframite samples analysed in this study versus mole % $FeWO_4$.

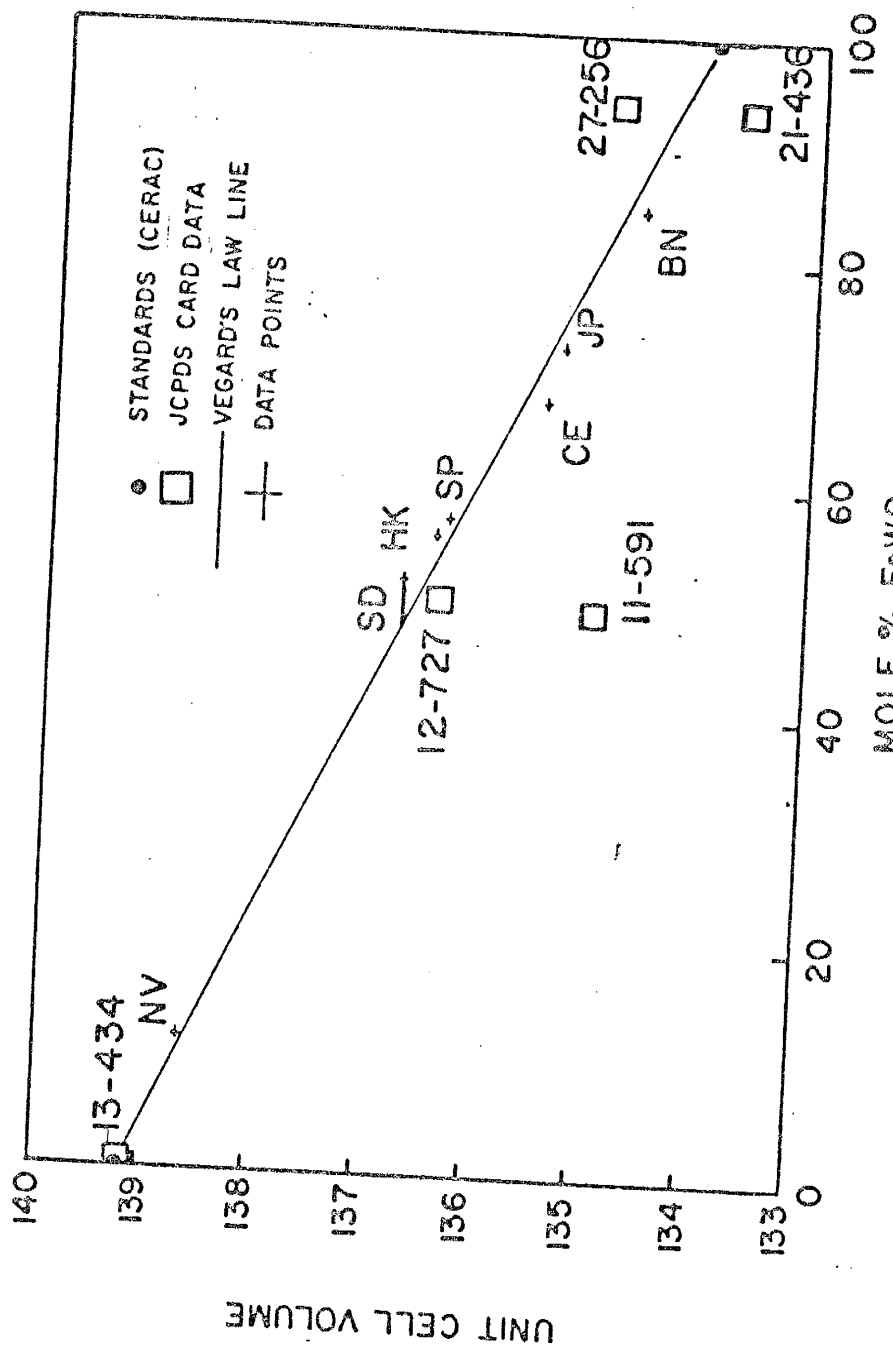
STANDARDS (CERAC)
JCPDS CARD DATA
VEGARD'S LAW LINE
DATA POINTS
13-434
NV
SD
HK
12-727
SP
CE
JP
11-591
BN
27-256
21-436
140
139
138
137
136
135
134
133
0
20
40
60
80
100
MOLE % FeWO4
UNIT CELL VOLUME

3) Variation of the crystal perfection

An estimation of crystal perfection can be roughly determined using the width of a diffraction peak at half height as the width increases with decreasing crystal perfection. A crystal's perfection diminishes with increasing strain and decreasing crystallite size. Deformation of the crystal structure due to the incorporation of non-stoichiometric cations and/or anions contributes to strain and small crystallite size. As a consequence, the diffraction peaks may broaden measurably.

The breadth of the (100) peak was used for this determination as it had no interference with surrounding peaks and is a sharp basal reflection and well defined. A comparison of the variation in peak width at half height with geochemical analysis (table 5) shows no obvious correlation.

GEOCHEMISTRY

Microprobe Analysis

Three wolframite samples were analysed using an X-ray Microprobe. Due to an improper standard and data reduction routine only approximate Fe/Mn comparisons between the examined sites could be made. The general results are as follows:

1) Panasqueira (PP): A traverse of this crystal indicated a very homogeneous composition throughout the core of the crystal with a composition of 80.7 mole % $FeWO_4$. A sharp increase in $FeWO_4$ content to 98.7 mole % $FeWO_4$ occured at the crystal edge.
2) Victorio Mts. (VM); An iron-poor sample showing only slight variation in Fe content (20.9 to 16.3 mole % $FeWO_4$) across a traverse of the crystal.
3) White Oaks (WO); A huebnerite sample which was surprisingly homogeneous showing no obvious variation in Fe content. All analysis points were 0.4 mole % $FeWO_4$.

   No high concentration of a non-stoichiometric element was found to explain the anomalous opacity of this sample.

X-ray Fluorescence Analysis

Fourteen wolframite samples were analysed using x-ray fluorescence spectrometry. The experimental conditions are listed in Appendix I.

Several samples contained an appreciable amount of quartz. These samples were 'normalized' to 0% SiO_2 in order to compare Fe/Mn/W concentration ratios with the other samples. The raw results and normalized results are listed in weight percent in Table 5. Sub-totals of the measured concentrations of the stoicheometric and non-stoicheometric elements (as oxides) are provided for comparison. The samples are listed in order of decreasing transparency. Dashed lines represent concentrations below the limits of detectability.

Neutron Activation Analysis

Ten samples of wolframite were analysed for trace and major elements using NAA. Elements are reported in ppm (table 5). Accuracy was +/- 25% as determined by concentrations of each element in known standards.

Table 5: Geochemical analysis of 14 wolframite samples. Samples are listed in order of decreasing transparency. Samples SD, CE, TT, SP, and JP contained high amounts of SiO_2. For these samples, FeO, MnO and WO_3 concentrations are listed as acctual measurements/and normalized without SiO_2.

	BP	PP	VM	NV	MO	BN	SD	CE	TT	HK	SP	JP	WO
WO3(X)	76.72	76.46	73.28	75.31	71.32	76.7	61.89/74.84	71.38/76.14	48.35/75.60	67.92	61.06/72.91	61.06/72.91	75.98
FeO(X)	0.074	20.29	7.43	2.44	4.77	19.16	9.78/11.83	14.92/15.91	12.47/19.49	11.84	11.75/14.03	17.27/17.64	0.16
MnO(X)	22.25	3.51	16.92	19.04	13.19	3.5	9.11/11.02	7.11/7.58	2.55/3.99	9.53	8.75/10.45	6.54/6.68	22.07
SUBTOTAL	99.07	100.3	97.6	96.7	89.3	99.4	97.7	93.4	99.9	97.2	97.4	99.7	98.21
SiO2(X)	0.41	0.47	0.87	2.63	0.82	1.05	17.29	6.11	36.61	8.17	16.07	2.28	1.78
Al2O3(X)		0.09	0.49	0.026	0.172	0.065	0.014	0.034	0.149	3.07	1.04	0.389	0.226
MgO(X)		0.24	0.31			0.38			0.009			0.308	
CaO(X)	0.027	0.03	1.27	0.63		0.99	1.8	0.09	0.19	0.914	0.19	0.067	0.352
Na2O(X)	0.043		0.01					0.009		0.005		0.009	0.011
K2O(X)	0.004	0.029	0.02	0.007	0.02	0.07	0.003	0.009	0.015	0.583	0.21	0.013	0.006
IN PPM													
Sc*	80	132	706	9	57	88	21	64	68		272	220	24
Cr(N)					330								
Co*	9		20	0.25			2	8	1	20	6	37	15
Ni*	107	112	114	101	104	259	79	98	74	186	90	195	146
Zn*	246	301	467	219	249	194	98	103	733	174	146	240	146
Pb(X)	4358	81	345	1097	101176	46	208	66	901	195	1350	106	59
Mo(X)	27	23	157				13	25		30		21	
As(N)	40				140								
Br(N)													
Sr(N)				1040			19						
Ag(N)				0.8	3								
Sb(N)				23					3.3				
Cs(N)	2		2		1.7		0.8	2					
Ba(N)					2.8		0.4	0.7	158		10		
La(N)											4200		560
Ce(N)	6		22	8.5	2.6		3.5	8.1	8.5		49		8
Eu(N)	0.2		0.5	2.2	0.6		0.3	0.6	0.5		99		4.3
Tb(N)				2	0.5		0.2	0.4	6.3		0.6		0.6
Yb(N)			423	64	5.3		7.2	7.5	3.2		53.1		0.3
Lu(N)			85	11			1				5		2.6
Hf(N)			6.6										1
Ta(N)		0.3	932	31	9.5		7	16	2		3.6		0.4
Th(N)				2					1.5		409		
U(N)	8		64	24					48		15		
											300		
TRANSPARENCY	7.3	6.7	6.5	5.3	4.5	4.5	4.3	4	0	0	0	0	0
d(100)	0.162	0.096	0.120	0.222	0.081	0.100	0.145	0.159	0.109	0.080	0.101	0.147	0.158

INTERPRETATION OF GEOCHEMISTRY

GEOLOGIC SETTING

Tungsten deposits have been grouped by Hess (1917) into six types; segregation deposits, pegmatite dikes, veins, replacement deposits, contact-metamorphic deposits and placers. Of all of these, vein deposits, more specifically quartz vein deposits, are the most common occurrence of wolframite

A table of the geology of each wolframite deposit along with a summation of the geochemical analysis from this study is found in table 6. Assuming the mineral assemblage is indicative of the variety of elements present in the ore fluids, it is not surprising that a rough correlation is found between the mineral assemblage found at each deposit and the geochemical analysis.

Table 6: General geology of each wolframite deposit.

SAMPLE LOCATION	REGIONAL STRUCTURES/TECTONICS	REGIONAL ROCK UNITS	OCCURENCE OF WOLFRAMITE	ORE ELEMENTS	MINERAL ASSEMBLEGE	GEOCHEMISTRY ppm or wgt %	AGE OF MINERALIZATION	COMMENTS	REFRENCES
TIPTOP, AZ TT	BRADSHAW MTS.		GRANITE AND PEGMATITE VEINS	Au, (W)		Zn 733 Pb 901 Sb 158			EMMONS, et al., 1906
BOLSA NEGRA BOLIVIA (BN)	CORDILLERA REAL STRUCTURAL PROVINCE		QUARTZ VEIN		Qtz, Tourmaline Wolf, Sch, Apy sulfides, fluorite	Ca 1%, SiO2 1.1% Ni 259 Zn 194	Lt. Triassic		KELLY & TURNEAURE 1970
SERRA de SAO FRANCISCO ESTAD de SAO PAULO BRAZIL (SP)			QUARTZ VEIN			Pb 1350, Zn 146 Sc 158, Ta 409 U 300, Ba 4200			
CORNWALL GREAT BRITAIN CE		CARBONACEOUS SHALES & MUDSTONE INTRUDED BY GRANITE	QUARTZ VEINS	Sn (W) Cu Zn Pb	Qtz, Cass Wolf, Apy Cpy, Tourmaline Sch, Fluorite	SiO2 6% Zn 103	Permian	MULTIPLE INTRUSIVE EVENTS WITH STOCKS SUPPLYING METALS FOR VEINS	TAYLOR & HOSKING, 1970 SAWKINS, 1966
NEEDLE HILL MINE, HONG KONG HK			QUARTZ VEINS			SiO2 36.61% Zn 174, Ni 186 Pb 195			
HANAOKA MINE JAPAN (JP)						Ni 195, Zn 240 Sc 220, Pb 106			
SILVER MINES MISSOURI (MO)	ST FRANCIS MTS. OZARK DOME	PREC GRANITE & PORPHYRY DIKES IN CAMBRIAN SEDS DOL SS SH CONG.	QUARTZ VEINS IN PRECAMBRIAN VOLCANIC CONTACTS	Ag Pb W Zn	Py, Gal, Sph Cpy, Sch, Topaz Fluorite, Stolzite cass, wolf	Pb 10.1% Zn 249, Ni 104 Cr 330, As 140	PRECAMBRIAN?	HYDROTHERMAL ASSOC WITH EMPLACEMENT OF GRANITE AND VOLCANICS	TOLMAN, C., 1933
BLACK PINE PHILLIPSBURG MONTANA (BP)	LEWIS AND CLARK OVERTHRUST	PREC SPOKANE SERIES AND BELT SERIES INTRUDED BY TERTIARY GRANITE	QUARTZ VEINS IN CONTACT METAMORPHIC AREAS	Au Ag Pb Cu W	Qtz, Huebnerite Tetrahedrite, Py Gal, Malachite	Pb 4358 Zr 246 N. 107	TERTIARY		EMMONS, WH, 1907
WHITE OAKS, NM (WO)	TERITARY STRUCTURE LOCATED ALONG PRECAMBRIAN LINEAMENT	TERTIARY MONZONITE INTRUDED INTO PALEO SEDS SS SH	QUARTZ VEINS	Au W	Qtz, Albite Fluorite, Py Tourmaline, Anhydr Huebnerite, Gold	Ba 560 Ni 146 Zn 146	TERTIARY		GRISWOLD, B. 1959 NORTHRUP, 1959
VICTORIO MTS. NM (VM)	BASIN AND RANGE	TERTIARY ANDESITE & GRANITE INTRUDED INTO VOLCANICS AND SEDS LS DOL	QUARTZ VEIN	Pb Zn Ag Au W Be	Qtz, Musc, Py Wolf, Beryl, Gold Fluorite Wolfenite	Zn 467, Ni 114 Pb 345, Mo 157 Sc 706, Ta 932 Yb 423	TERTIARY	ZONED HI-SILICA FRACT. PLUTON OR SHALLOW GRANITIC SOURCE	THORMAN & DREWES, 1980
NEVADA (NV)		GRANITE PORPHYRY INTRUDING CAMBRIAN	QUARTZ VEINS	W Au Ag	Qtz, Huebnerite, Fluorite, Py, Sch	Zn 219, Ni 101 Sr 1040 Pb 1097	POST CARBONIFEROUS	GRANITIC STOCK WITH MAGNATIC WATERS DEPOSITING	WEEKS, FB 1908
SAN CRISTOBAL PERU (SC)	MESOZOIC FOLD BELT OF THE ALTIPLANS STRUCTURAL PROVINC YAULI DOME	QTZ MONZONITE IN PALEOZOIC & MESOZOIC SEDS LS SS	QUARTZ-BASE METAL VEINS	W Cu Zn Pb Ag	Augelite, Musc, Py Wolf, Qtz, Cpy Sph, Galena, Barite, Carbonates		TERTIARY	HUEBNERITE	
PANASQUEIRA PORTUGAL (PP)		LT. HERCYNIAN AGE GRANITE INTRUDING LT PREC. SCHISTS	QUARTZ VEINS	W Sn	Wolf, Tetrahedrite Sph, Galena Qtz. Fluorite Sericite Py, Carbonates	Zn 301, Ni 112 Pb 345, Mo 157 Sc 132, Yb 423 Ta 932		WOLFRAMITE ASSOC WITH METEORIC WATER IN HYDROTHERMAL SYS	
LAWRENCE COUNTY SOUTH DAK (SD)	BLACK HILLS	PREC GRANITE PEGMATITIC INTRUSIVE IN ALGONKIAN SCHISTS	W REPLACEMENT IN A SANDY DOLO	W (Sn)	Wolf, Tourmaline Musc, Cass, Qtz Albite, Fluorite Barite, Gypsum, Py	SiO2 17.2% Pb 208			

EXAMINATION OF HYPOTHESIZED FACTORS FOR INFRARED TRANSPARENCY CONTROLS

Several suggestions were hypothesized as possible factors controlling infrared transparency. Each of these suggestions can now be analysed in light of the data obtained from this study.

1) Crystallographic control:

The wolframite crystal from Panasqueira had excellent crystal habit and was large enough for crystallographically oriented sections to be made. Sample WP0 was cut along (001), (010), and (100) and observed for transparency variations. No variation in the transparency was noted. The Victorio Mountains section which had variable transparency to begin with also showed no change in transparency with crystallographic orientation.

No correlation existed between degree of crystal perfection and composition. The crystal perfection is not sufficiently altered by the presence of extraneous elements present in ppm concentrations. This independence is observed when comparing geochemical analysis with variations in peak width at half height as in table 5.

2) Major element compositional control:

The predominant control of transparency for wolframite in the visible spectrum has been said to be the iron content where an increase in the iron content corresponds to a rapid decrease in transparency. In visible light only the extremely iron-poor huebnerite is transparent.

This relationship does not hold true in the infrared where iron content seems to be independent of infrared transparency. Both Panasqueira (PP) and San Cristobal (SC) are iron-rich wolframites (85% and up to 94% $FeWO_4$ respectively) yet they both are transparent in the infrared. Conversely, White Oaks (WO) is a manganese-rich wolframite that is opaque in the infrared. Figure 4 is a plot of mole % $FeWO_4$ versus transparency. The random distribution of the data points indicates that transparency is independent of iron content. This is supported by Carmical (1984) who reports that the infrared absorption edge of ferberite exists at 16,000 A, far beyond the infrared window used in this study.

Figure 4: Mole % $FeWO_4$ plotted against transparency. Transparency is independent of iron content.

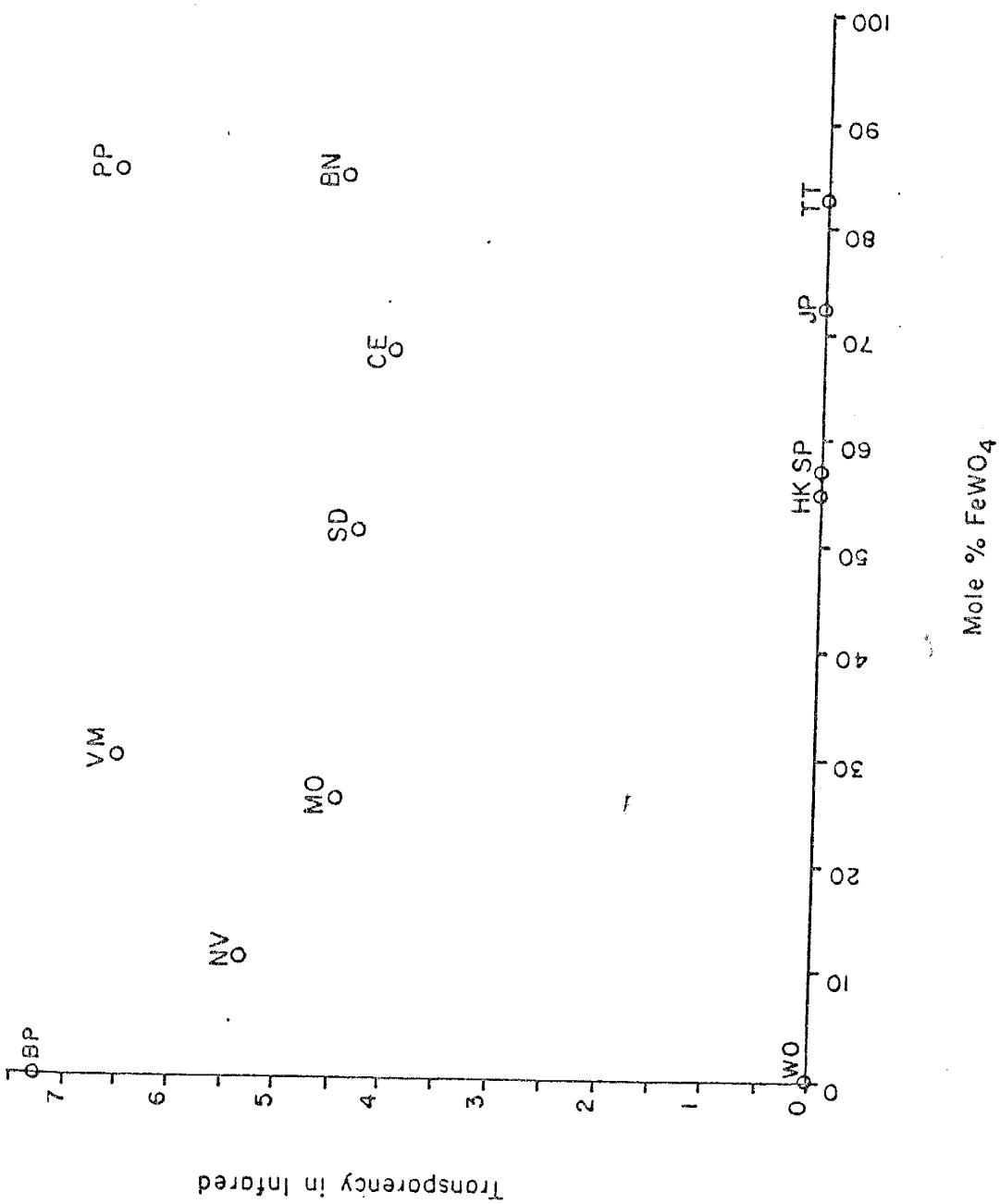
Transparency in Infrared
Mole % $FeWO_4$
WO
BP
NV
MO
VM
SD
CE
BN
PP
HK SP
JP
TT
0
10
20
30
40
50
60
70
80
90
100
1
2
3
4
5
6
7

3) Trace element control:

All wolframites analyzed contained a variety of trace constituents in varying amounts. In determining which elements do not exhibit a control on transparency, the following criterion was developed:

a) A plot of each element's concentration versus transparency was made. Those elements which were in high concentration in the transparent wolframites were eliminated as they could not exhibit a detrimental effect on transparency. These elements include: Pb, Sr, Sc.

b) Those elements which were contained by a separate phase were disregarded. This included, SiO_2, Al_2O_3, CaO, Na_2O, K_2O, MgO, As, Sb, Ag, and the REE. These elements are incorporated into the minerals quartz, feldspars, scheelite, chlorite and various sulfides. Separate phases were determined using XRD and their association with wolframite in hand samples. Most samples contained quartz as the only separate phase.

The sample, Silvermines (MO) was found to have an extremely high lead content of 11%. The concentrations of the major oxides FeO + MnO as well as WO_3 were less than the stoichiometric values (ie 23.6 vs 18 and 76.4 vs 71.3% respectively). X-ray diffraction data suggested the presence of the lead-tungstate stolzite ($PbWO_4$) as well as

wolframite in this sample. These are present as separate phases and not as a solid solution. Stolzite has been reported at this locality as well as argentiferous galena which is also very common (Tolman, 1933). No other sample contained such an anomalously high concentration of another mineral phase.

c) Elements which were only observed in one or two wolframites were considered to be unimportant in controlling of transparency for wolframites in general. They could, however, be a factor in the wolframite(s) they are present in. They were set aside for use in explaining variations in transparency between otherwise geochemically identical wolframites. These elements include Ba, U, Th, Br, and Cs.

Those elements which remained (Cr, Co, Ni, and Zn) were looked at to determine compatibility in the wolframite structure. The criteria considered included "ionic" radii of the substituting species, electronegativities, site compatibility and preference, and the energies of the replacement process. Available sites for substitutions in the wolframite structure include the lattice sites for tungsten (W^{+6}), oxygen (O^{-2}) and Fe/Mn (Fe^{+2}/Mn^{+2}) or into the vacant octahedral positions, provided that overall charge neutrality is preserved.

Figure 5 presents a correlation of the concentration of the transition elements, Ni, Cr, Co and Zn with transparency for those wolframites which are transparent. There also exists the more generalized separation of transparent and opaque wolframites. These two populations have similar transition element concentrations. It would seem that transition elements can alter the transmission of infrared light to a small degree, roughly analogous to there effect in visible light where such elements cause darkening in minerals such as cassiterite and sphalerite. Superimposed upon the transition element trend is a larger, separate process which produces total absorption of the infrared wavelengths used in this study. This overriding control of transparency does not seem to correlate to the presence of any of the elements analysed for in this study. It can only be summarized that the geochemical control of infrared transparency/opacity in wolframite has yet to be determined.

Figure 5: A plot of transition element concentration versus transparency.

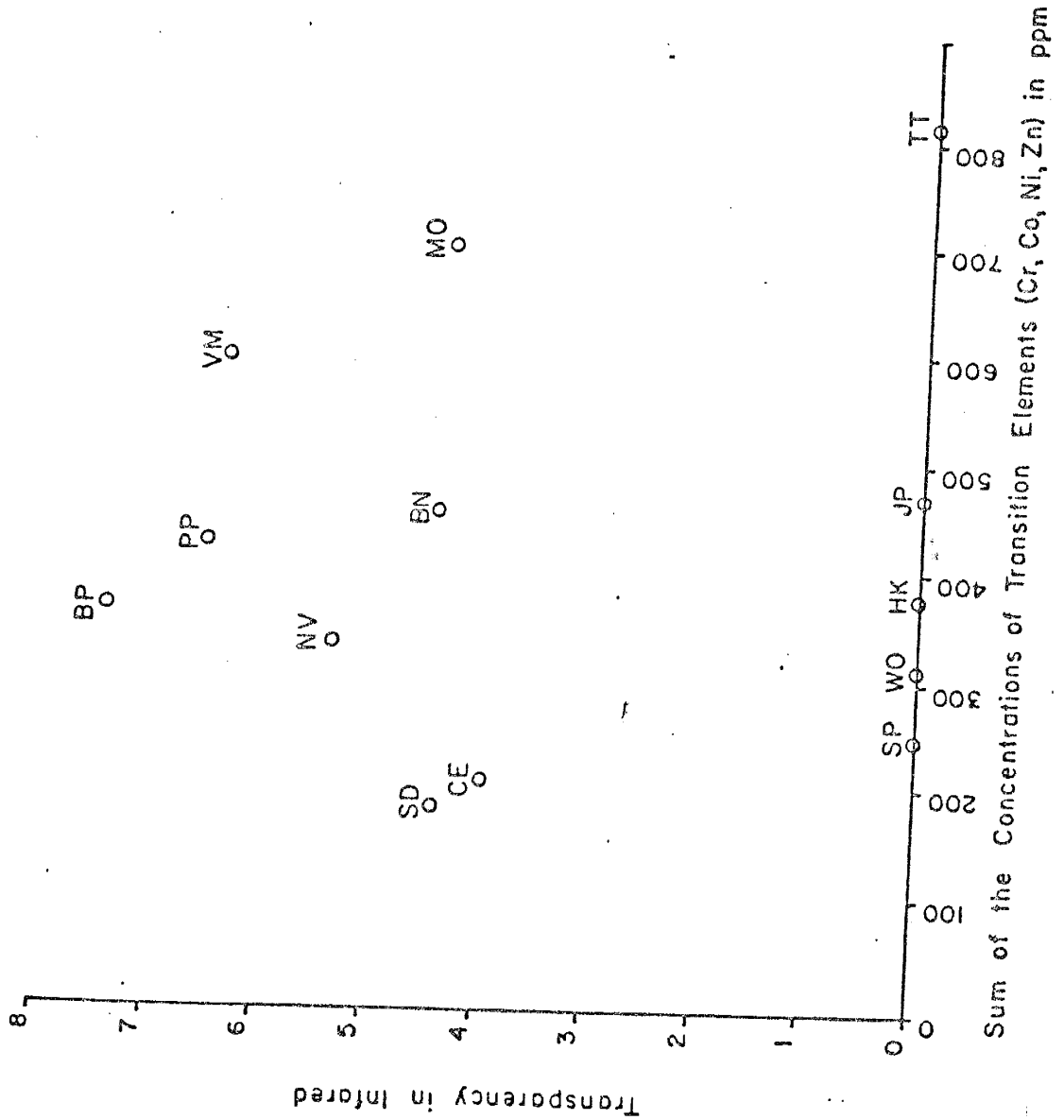
Transparency in Infrared
Sum of the Concentrations of Transition Elements (Cr, Co, Ni, Zn) in ppm
0
1
2
3
4
5
6
7
8
0
100
200
300
400
500
600
700
800
BP
PP
VM
MO
BN
NV
SD
CE
SP
WO
HK
JP
TT

CONCLUSIONS

The original hypothesis of this study was that geochemistry must control infrared transparency in the mineral wolframite. The elements suspected to exert this control were hypothesized to be iron or one of the many trace elements which have been routinely found in wolframite geochemical analysis. Several analytical techniques were used to approach this problem.

Geochemical analysis of the wolframites were done using XRF and NAA. The results were compiled and compared to infrared transparency. Many elements analysed for seem to have no correlation between their concentration and sample transparency. However, the concentration of the transition elements did have an observable negative influence on infrared transparency.

The substitution of these elements into the Fe/Mn octahedral site must cause a change in the electronic configuration of the wolframite structure. The correlation of transition element content with coloration in visible light is also well documented for cassiterite (SnO_2).

X-ray diffraction was used to determine the mineralogical purity of wolframite samples as well as the amount of variation of unit cell parameters in natural

wolframites and to try and relate this variation to trace element composition. Most samples conformed to Vegard's law. Those which plotted off the calibration curve had only a slight variation which was equivalent to the effect of increasing or decreasing their $FeWO_4$ content by <5 mole %. As many previous studies of wolframite have assumed that the cell dimension variations are linear, this change is considered significant. The ppm concentrations for all the extraneous elements found in the analysis of these wolframites does not seem to be significant enough to create such a deviation of the cell volume. This variation must be the result of an as yet undetermined geochemical constituent.

A further study must be undertaken to expand the sample base and to expand the analysis of natural wolframites. A possibility which is now being examined is trivalent iron or manganese balanced by hydroxyl in the wolframite structure. Water is a common constituent of most wolframite analysis and may well have a strong influence on wolframite infrared absorption.

SECTION II

FLUID INCLUSION ANALYSIS

This aspect of the study is an attempt to address the validity of the common assumption in ore deposit studies that microthermometric data obtained from transparent gangue can be used to understand conditions of ore deposition. The relationship between the physical and chemical conditions for wolframite and quartz deposition will be examined using wolframites from the four deposits which contain sufficiently transparent samples.

Bailly (1938 and 1942) measured optical properties of various opaque minerals using infrared light. Neither of these studies addressed any petrologic applications of infrared microscopy. The problem of the genetic relationship between ore and gangue has been addressed by Moore and Moore (1979). They examined the Cornwall district in Great Britain comparing fluid inclusion data obtained from cassiterite to that obtained from quartz and found a large discrepancy (cassiterite Th=360-420, quartz Th=280-380^{o}C). Their study points out the obvious limitation to fluid inclusion studies which rely solely upon transparent gangue minerals.

Sample Preparation

Doubly polished thick sections of wolframite samples were made using the technique of Holland et al. (1978). Due to the dependency of transparency on thickness, some wolframite sections needed to be much thinner than the standard 300 microns for fluid inclusion sections. In order to determine the necessary thickness for infrared transparency yet avoid the time consuming chore of polishing a section to completion, the sample was broken into cleavage chips. Due to wolframite's excellent cleavage along {010}, it forms well developed flat plates with sufficient natural 'polish' to be used in fluid inclusion studies. The Fe-Mn content changes the crystal morphology somewhat and alteration affects the hardness and friability but in general most samples yielded usable cleavage chips. Petrographic observations of these chips in the infrared quickly determined how thin the sample must be to transmit infrared light. Of the samples in this study only samples from Panasquiera (PP) and the Victorio Mountains (VM) were sufficiently transparent to use the standard 300 micron thick sections. All other samples needed to be thinner, in the order of 50-150 microns. Due to the thinness of these wolframite sections, extra care must be used to prevent crumbling in removal of the sections from the slide. A paint brush was used to facilitate removal of the remnant film of epoxy on the sections.

Calibration

Heating and freezing measurements of fluid inclusions were made using a gas flow type heating/freezing stage manufactured by Fluid Inclusion Inc. stage (Roedder, 1984) with the Research Devices Infrared Microscope. Careful calibration of this stage was done using the fusion point of eight solids in the temperature range of +80 to +455^{o}C. The calibration of the temperature range of -60 to +0^{o}C was done by using the melting point of pure water as well as CO_2. Liquid CO_2-rich inclusions were carefully examined to determine the effect, if any, of CO_2 absorption of infrared radiation. CO_2 absorbs strongly in the range 7-7.7 microns (Weast, 1978). No variation in the melt temperature or temperature of homogenization was noted when measured with the infrared light source. CO_2 inclusions melted at -56.5^{o}C +/- 0.2 and homogenized at +26.7^{o}C +/- 0.6.

Homogenization was determined by the temperature of the last visible reversible phase change of the inclusion. Salinities are reported as equivalent weight percent NaCl. They were calculated from freezing point depression of the fluid inclusion using the equation determined by Potter et al. (1978).

The first step in examining fluid inclusions was to compare fluid inclusion data measured with the infrared light source to that measured with the visible light source.

The Linkham freezing/heating stage was used for visible light measurements. This comparison encompassed three data sets.

1) Chemical standards with known melting temperatures were used to calibrate each stage. Overall, the calibration curves for both stages show excellent agreement with the accepted melting temperatures and with each other (table 7).

TABLE 7

VISIBLE CALIBRATIONS (C)	INFRARED CALIBRATIONS (C)	ACTUAL MELT MELT TEMPS. (C)
81-88	81.8-82.1	81-83
112-116	114.7-115.3	114-116
132-136	135.1-135.5	134-136
162-167	164.3-165.5	164.5-166.5
189-192	190.5-192	190-193
	395-399	398
	453-456	455

2) Huebnerite from the Black Pine mine in Montana (BP) is transparent to both visible and infrared light so fluid inclusions from this sample were measured using both light sources. A CO_2-rich fluid inclusion from quartz at the Victorio Mountains deposit was examined using both light sources. Figure 6 plots the visible light measurements against the infrared light measurements. This plot shows the close agreement of the measurement sets with each other.

3) A pure H_2O standard and a CO_2 standard were analysed for freezing temperatures using both light sources and these data points are also plotted on figure 6. No variation in the melting temperature of either substance was noted between measurements made with both light sources.

In all three comparison sets, no systematic difference was found between the two stages or the two light sources.

Figure 6: Plot of quartz and huebnerite temperatures of homogenization and salinities determined from pure H_2O and CO_2 measured with infrared light versus visible light. No systematic variation is evident.

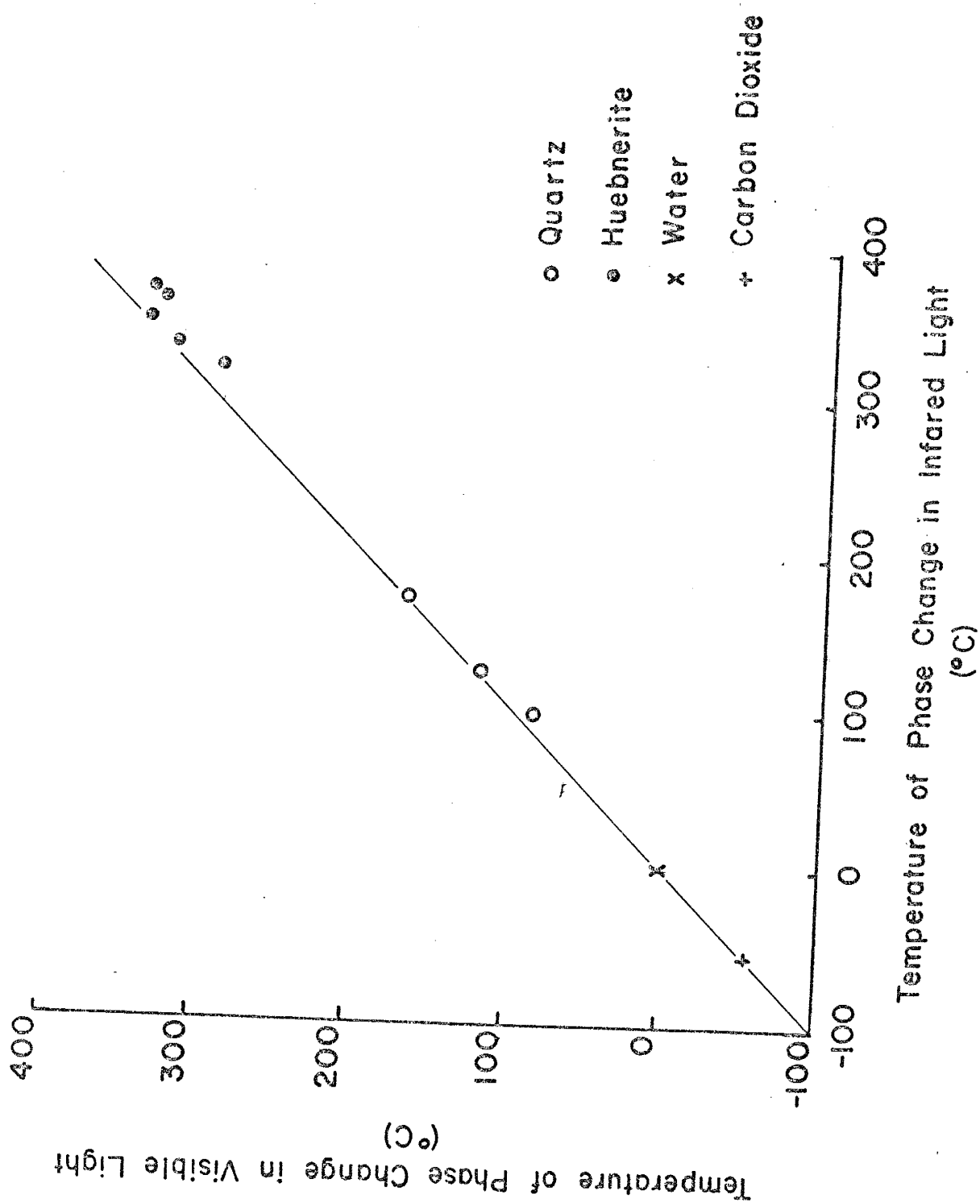
Temperature of Phase Change in Visible Light (°C)
400
300
200
100
0
-100
-100
0
100
200
300
400
Temperature of Phase Change in Infared Light (°C)
o Quartz
• Huebnerite
x Water
+ Carbon Dioxide

General Observations of Fluid Inclusions

Fluid inclusion were found in every transparent wolframite sample although the quantity and quality varied. Inclusions were classified as primary, pseudosecondary and secondary according to the system developed by Roedder (1984).

It was found that cleavage chips provided the best sections for fluid inclusion study possibly because the fluid inclusions seemed to be preferentially oriented along the cleavage direction. No doubt this was due to the growth of wolframite as the orientation of the growth surface controls inclusion entrapment. Secondary inclusions were easily noted as they occurred in planes cutting the crystal at all angles.

Panasqueira, Portugal (PP)

Wolframite from the Panasqueira, Portugal deposit was exceptionally transparent in the infrared even in extremely thick cleavage chips. Each section contained numerous fluid inclusions suitable for measurements. Unfortunately, the wolframite sections became progressively opaque upon heating. Most sections were opaque by 200^{o}C, before any inclusions were homogenized. The temperature of opacity was recorded as it represented a minimum temperature above which

temperatures of homogenization must occur. Fluid inclusions from the Fe-rich wolframite at Panasqueira are of three types.

TYPE I: By far the most abundant type of fluid inclusion, type I constituted greater than 60% of the total fluid inclusion population. These are simple two phase (liquid-vapor) inclusions with vapor >75% by volume and most often >95%. Sizes ranged from 10-30 microns in the long dimension. Little or no observable liquid wets the walls of these inclusions. Seen as opaque stringers and interlocking groups. Few had enough observable liquid to provide qualitative information (figure 7).

TYPE II: Type II inclusions are much less common than type I. They are primary two phase inclusions with liquid >70% by volume. A couple were observed to contain liquid CO_2. On the average, sizes range from 40-60 microns in the long dimension and 10-20 microns in width. Type II inclusions are commonly isolated although areas occur where types I and II occur together. The inclusion shapes are irregular to elongated ellipsoidal. The inclusion fluid is highly refractive giving the inclusion the appearance of having thick dark walls. Most qualitative information was derived from type II inclusions (figure 8).

TYPE III: Type III inclusions are secondary and are primarily liquid filled with little or no vapor phase present. These inclusions appear to be associated with healed fracture planes within the wolframite. Sizes range from 100 micron to <10 microns. They have a flat, two dimensional appearance and little or no refraction at the inclusion walls.

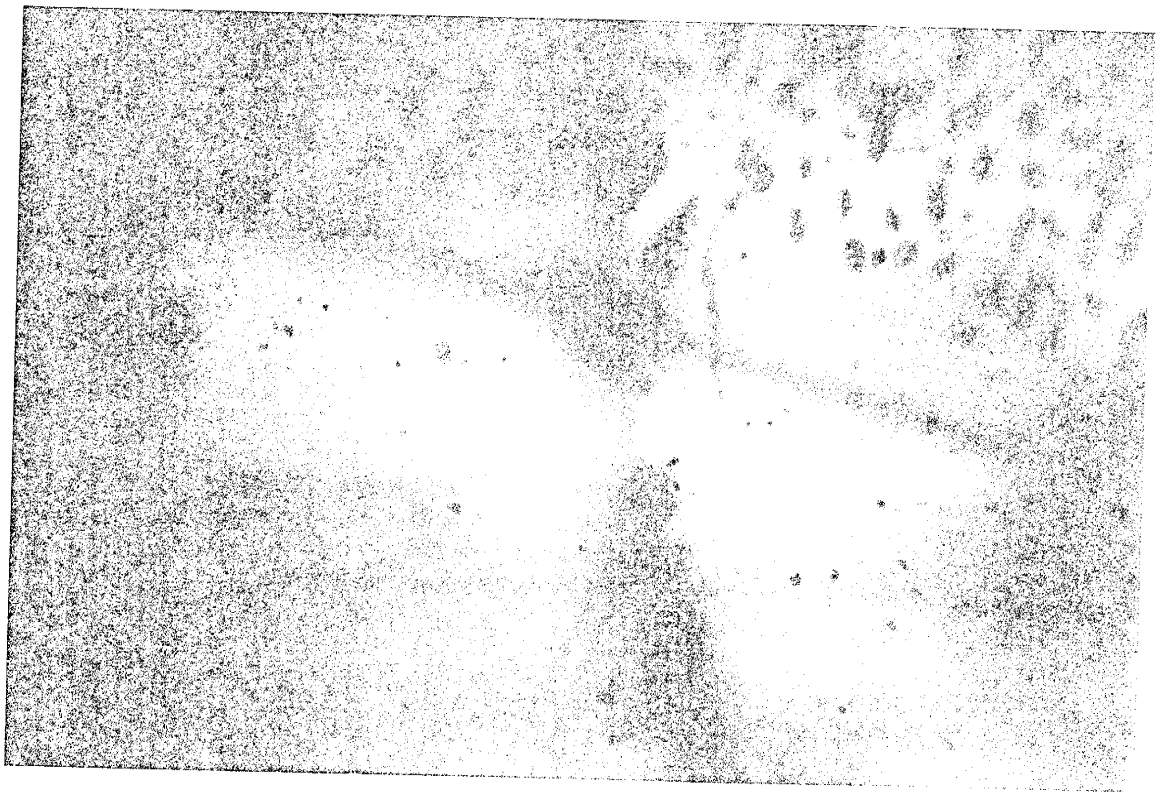

Figure 7: Vapor-rich type I inclusions aligned along banding in a Panasqueira wolframite cleavage chip. Inclusions are 10 to 15 microns in size.

Figure 8: A large (70 micron) liquid-rich two phase type II inclusion from Panasqueira wolframite.

Victorio Mountains, New Mexico (VM)

Fluid inclusions in wolframite from the Victorio Mountains deposit were not as numerous as the inclusions in quartz from the same samples. They averaged one or two measurable inclusions per chip. As no previous fluid inclusion studies had been done on this deposit, the quartz was carefully examined for detailed fluid inclusion data.

Fluid inclusions in the wolframite from the Victorio Mountains are of three types:

TYPE I: Type I are primary two phase (liquid-vapor) inclusions with liquid>vapor. The vapor phase is of variable volume, usually <20% total. One inclusion was noted that contained CO_2 liquid. No data was obtained from this inclusion. The inclusion fluid is highly refractive producing heavy shadows at the inclusion walls. The inclusions are irregular to ellipsoidal or more rarely in pseudo-cubic shape with sizes ranging from 50-60 microns long and 10-30 microns wide (figure 9).

TYPE II: Type II inclusions are irregular stringers and clusters of inclusions which appear opaque. Whether they are gas filled or liquid is unknown. They are usually small with a range of size from 50 microns down to <5 microns (figure 10).

TYPE III: Type III inclusions are secondary inclusions which are liquid rich and in places are only a single phase. Their fluid has a low index of refraction and their sizes have a great range from 70 to <10 microns (figure 11).

Fluid inclusions in quartz are of three types.

TYPE I: Type I inclusions are primary two-phase inclusions which are liquid rich. They are usually in various stages of necking down. Size ranges from 50 microns down to the limits of distinction. They are usually found within the center of quartz crystals (figure 12).

TYPE II: Type II inclusions are three-phase primary inclusions with H_2O-rich liquid, vapor and CO_2 liquid. They occur in clusters with signs of extreme necking down creating a large range in sizes from 100 microns down to 20 microns with the smaller sizes being average. The amount of CO_2 varies considerably. These inclusions are found in only 2 sections and are closely associated with vapor-rich (>75%) inclusions and type I inclusions (figure 13).

TYPE III: Type II inclusions are secondary two phase (liquid-vapor) inclusions with liquid>vapor. These inclusions are extremely small <10 microns and are always associated with secondary fracture planes within the quartz. These fracture planes are extremely numerous and in places give the quartz a milky opaque color.

Figure 9: A large (50 micron) liquid-rich type I inclusion in a wolframite cleavage chip from the Victorio Mountains deposit.

Figure 10: Vapor-rich type II inclusions ranging in size from 10 to 50 microns. Picture taken in a cleavage chip from the Victorio Mountains wolframite.

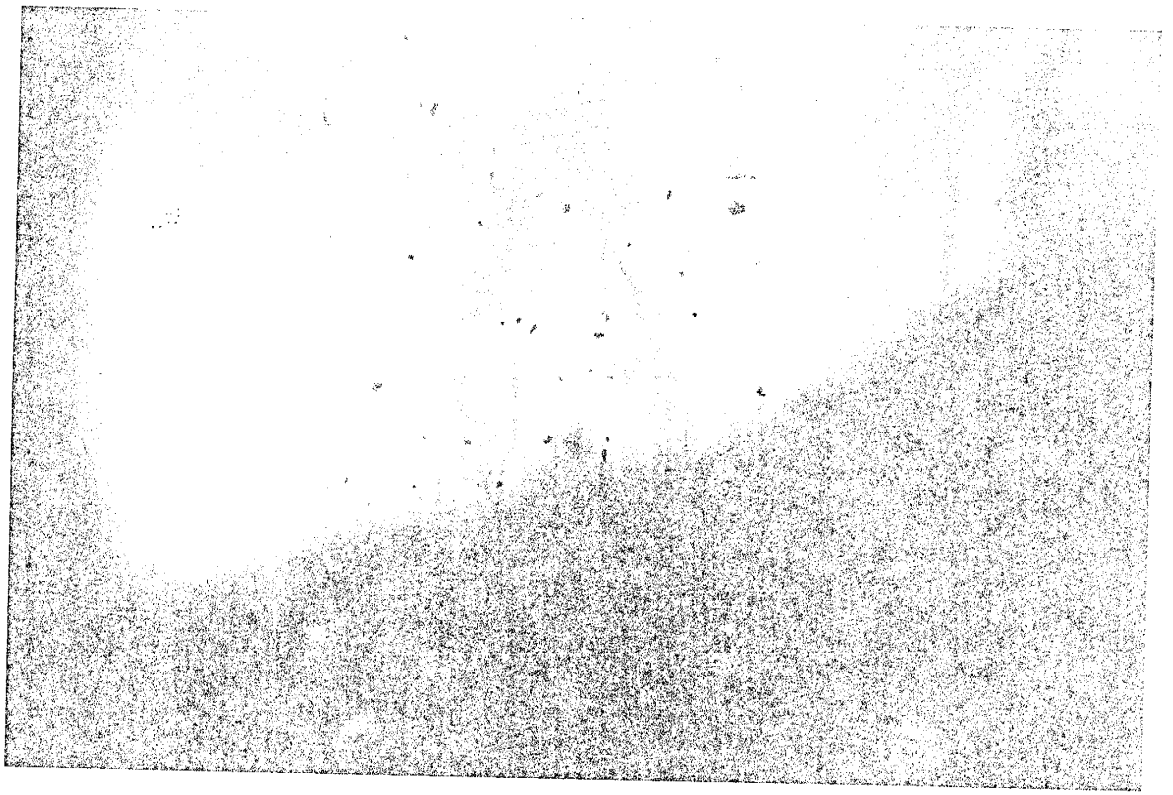

Figure 11: A field of small (<10 microns) secondary liquid one-phase type III inclusions found in wolframite from the Victorio Mountains deposit.

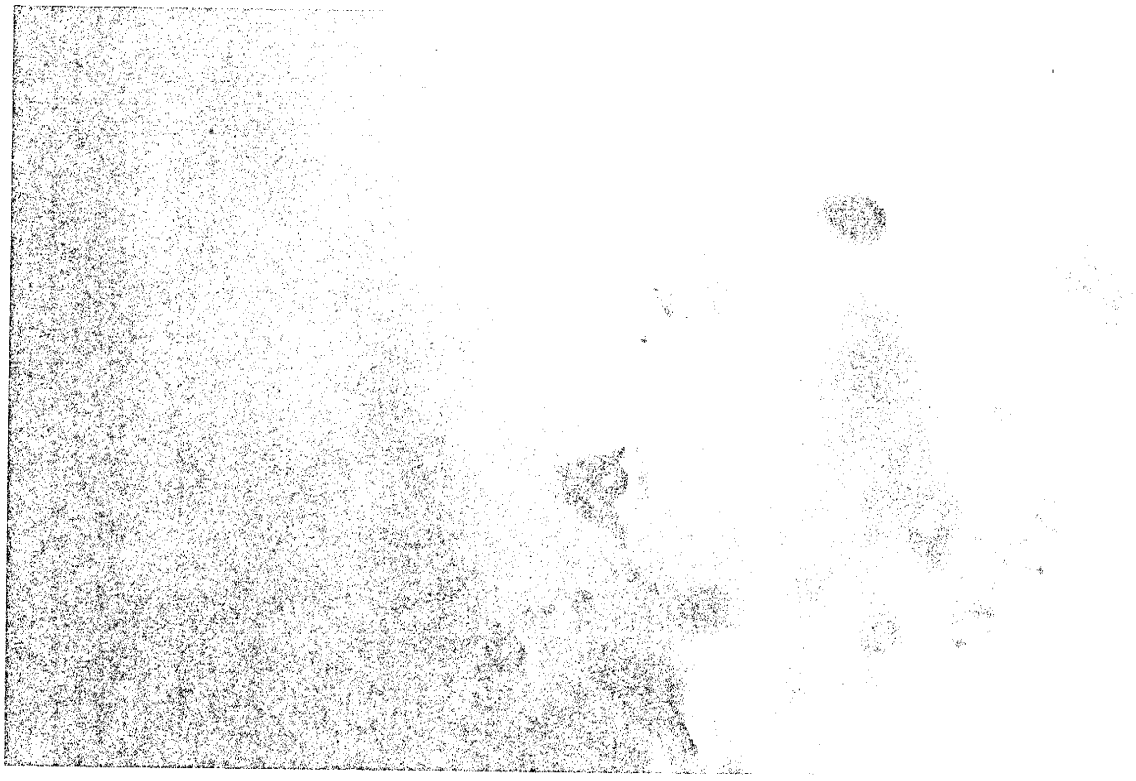

Figure 12: An isolated liquid-rich two phase type I inclusion in quartz from the Victorio Mountains deposit.

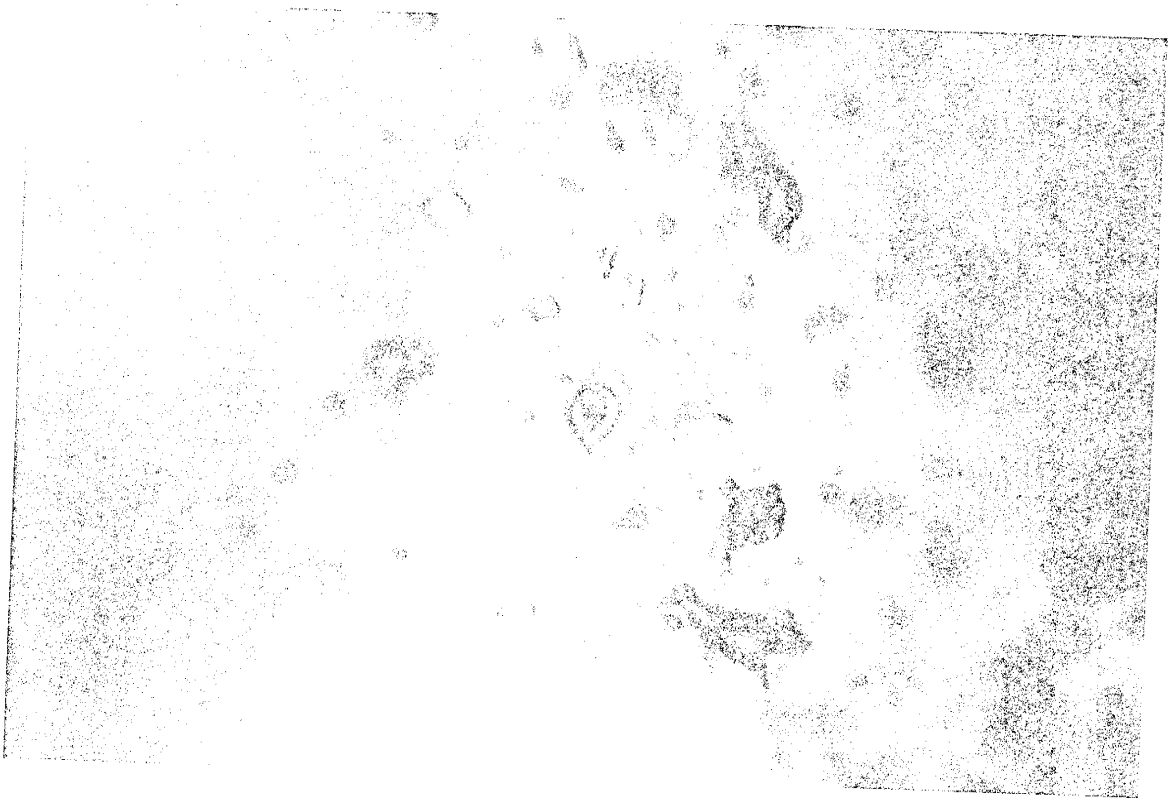

Figure 13: Association of vapor-rich and CO_2-rich type II inclusions in quartz from the Victorio Mountains deposit.

San Cristobal, Peru (SC)

The wolframite from San Cristobal is always transparent but only in the thinnest sections. Due to the extreme thinness of the sections many inclusions were lost. It was very difficult to find measurable inclusions which limited the amount of data obtained from wolframite.

Fluid inclusions from the Fe-rich wolframite at San Cristobal are two phase (liquid-vapor) with liquid>vapor. They have been grouped into two types.

TYPE I: Type I are primary inclusions, two phase, liquid-rich with vapor <20%. These inclusions appear to be flat with little refraction at the walls. They are generally shaped in a pseudo-cubic habit with an average size of 40 microns (figure 14).

TYPE II: Type II inclusions are secondary inclusions which always delineate fracture planes within the wolframite. They are usually too small, <10 microns, to determine separate phases.

Quartz from San Cristobal contains numerous two phase inclusions. Most inclusions appear to be primary or pseudosecondary and are aligned perpendicular to crystal faces. The majority are too small, <5 microns, for fluid inclusion analyses. These small primary and pseudosecondary inclusions are so dense they tend to make the edges of the

quartz crystals dark. However, within the center of most quartz crystals are clear areas which contain large, 40-100 micron long, isolated two phase primary inclusions usually irregular to elongate in shape. They exhibit no heavy refraction along the inclusion edges. Some have small highly refractive daughter phases which were too small to identify.

Figure 14: A large (200 micron) liquid-rich primary type I inclusion in a wolframite chip from San Cristobal.

Black Pine, Montana (BP)

Fluid inclusions in the huebnerite at Black Pine are of two types.

TYPE I: Type I are primary two phase inclusions liquid-rich which vary in size from 10-120 microns and are generally isolated. Some occur in small clusters with elongate shapes parallel the c-axis. They contain highly refractive fluid producing thick dark walls (figure 15).

TYPE II: Type II inclusions are single phase secondary inclusions which occur in planes of dense populations. Most are vapor-rich two phase inclusions cutting across crystal boundaries with sizes ranging from 30 microns to <5 microns.

The quartz from Black Pine has a milky appearance due to the density of minute fluid inclusions. Solid inclusions of huebnerite are present within the quartz.

Primary fluid inclusions are of two phases (liquid>vapor) and are isolated. Many have inverse crystal shapes with sizes ranging from 20-50 microns.

Numerous secondary inclusion are present in the quartz. They are generally small <5 microns. No measurements were determined from these secondary inclusions.

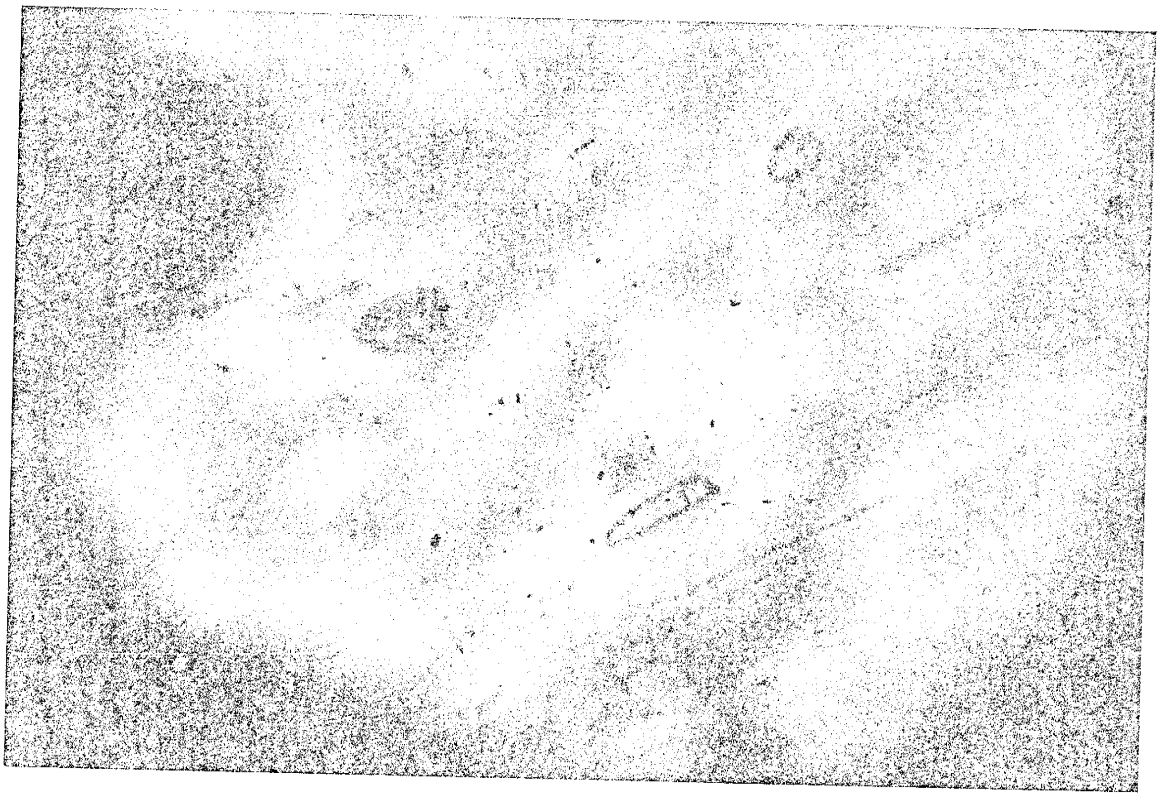

Figure 15: Primary two-phase type I inclusions in huebnerite from the Black Pine Mine. Sizes are about 20 microns.

Fluid Inclusions Microthermometry

Panasqueira, Portugal (PP)

Temperatures of homogenization were unobtainable as a decrease in transparency occurred with heating in these wolframites. This interesting phenomenon was reversible with cooling. The inclusions were not homogenized by the time the sample became opaque.

Salinities were determined from the type II inclusions in wolframite from Panasqueira. Most fluid inclusions froze between -40 and -75°C but all were frozen down to -100°C. Fluid inclusions in wolframite had a range of freezing temperatures from -10.9 to -4.8°C corresponding to 14.9 to 7.6 equivalent weight percent NaCl.

Victorio Mountains, New Mexico (VM)

Temperatures of homogenization and salinities are illustrated in Figure 16a and b. Type I liquid-rich fluid inclusions in wolframite homogenized to a liquid at temperatures ranging from 280 to 380°C. Most fluid inclusions which were suitable for heating studies were unsuitable for freezing due to extreme refraction along the inclusion walls and lack of visible hydrohalite formation. Those freezing temperatures obtained range from -3.3 to -5.8°C which correspond to 5.4 to 8.9 equivalent weight

percent NaCl.

The H_2O-rich type I inclusions in quartz homogenized to a liquid at temperatures ranging from 141 to 320°C. The CO_2-rich type II inclusions homogenized to a liquid at temperatures ranging from 210 to 317°C. One gas rich type II inclusion homogenized to a vapor at 262°C. Salinity measurements were made for both type I and type II inclusions. The CO_2 salinities were determined from the disappearance of the CO_2 clatherate (Collins, 1979). Salinities ranged from 1.3 to 10 equivalent weight percent NaCl with the CO_2 inclusions being the least saline.

Figure 16a: Temperatures of homogenization for wolframite and quartz from the Victorio Mountains deposit.

Figure 16b: Salinities versus temperatures of homogenization for the quartz and wolframite from the Victorio Mountains deposit.

Victorio Mountains

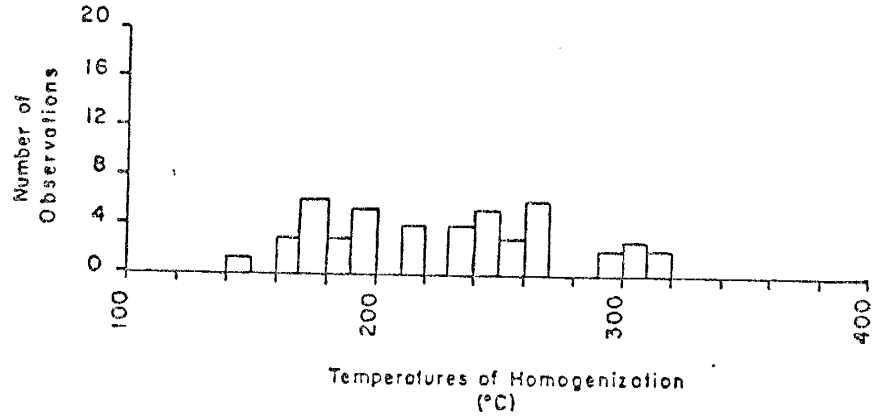

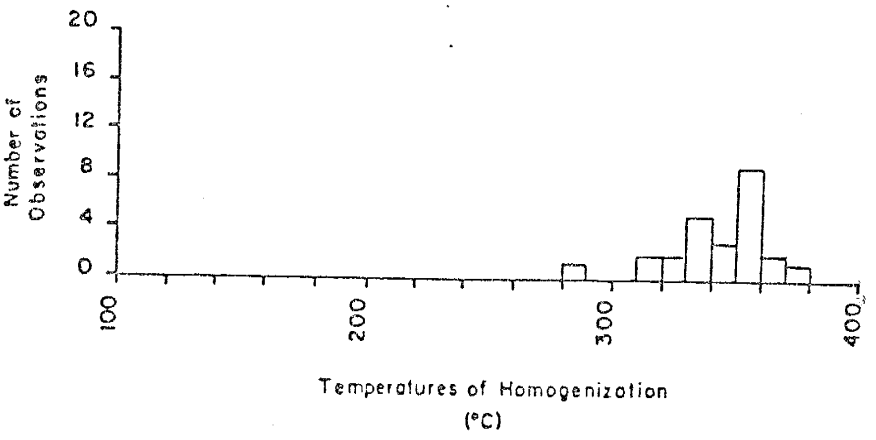

A

x=Quartz
o=Wolframite
Δ=CO_2 Quartz

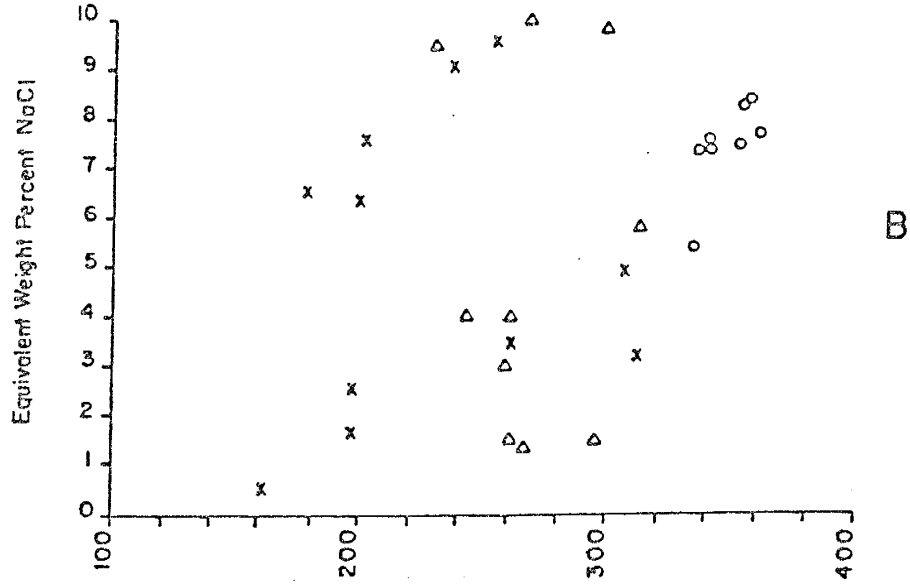

B

San Cristobal, Peru (SC)

Temperatures of homogenization and salinities from the type I liquid-rich inclusions in wolframite and quartz are illustrated in figure 17a and b. Type I inclusions for wolframite filled to a liquid with homogenization temperatures for primary inclusions ranging from 195 to 330°C with a mean of 270°C. Temperatures of homogenization determined from quartz range from 200 to 280°. Freezing temperatures from both minerals ranged from -0.9 to -4.1°C corresponding to 1.6 to 6.6 equivalent weight percent NaCl.

Figure 17a: Temperatures of homogenization for quartz and wolframite from the San Cristobal deposit.

Figure 17b: Salinity versus temperatures of homogenization for quartz and wolframite from the San Cristobal deposit.

San Cristobal

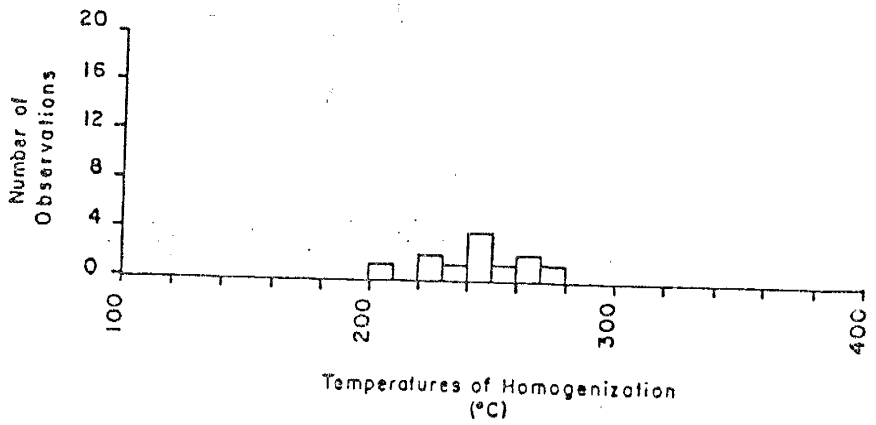

Quartz

A

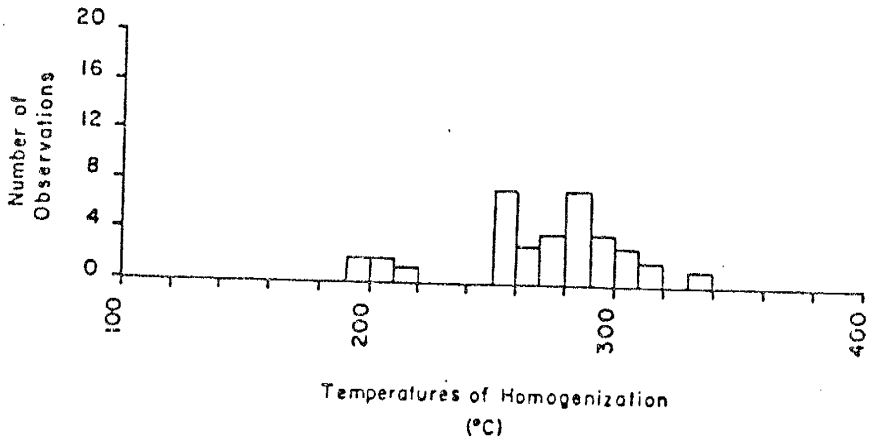

Wolframite

x=Quartz
o=Wolframite

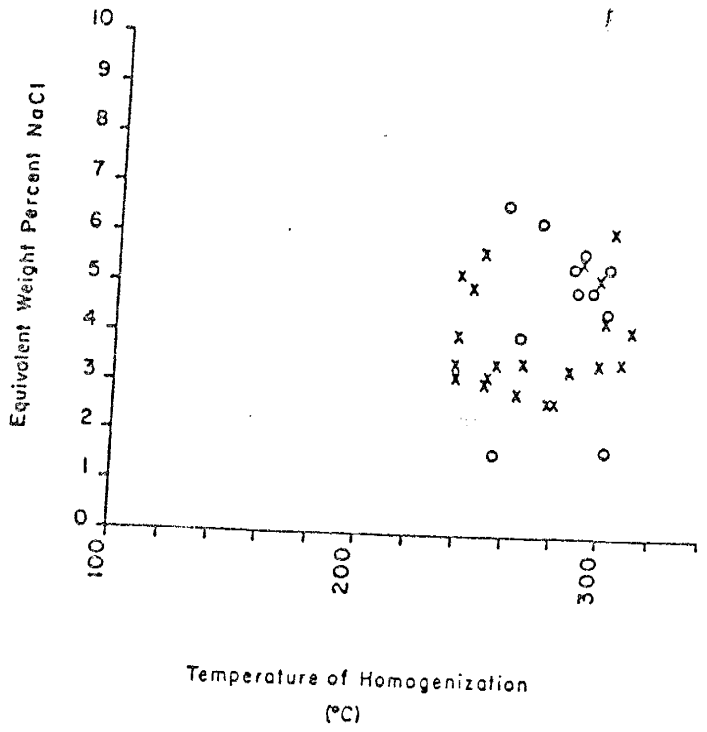

B

Black Pine, Montana (BP)

Temperatures of homogenization and freezing temperatures are illustrated in figure 18a and b. Type I liquid-rich inclusions from huebnerite homogenized to a liquid in the range of 210-280°C. Salinities ranged from 5.1 to 8.1 equivalent weight percent NaCl. Quartz homogenization temperatures range from 252-274°C. A single salinity measurement was made at -2.7°C which corresponds to 4.7 equivalent weight percent NaCl.

Figure 18a: Temperatures of homogenization for huebnerite and quartz from the Black Pine deposit.

Figure 18b: Salinity versus temperature of homogenization from quartz and huebnerite and quartz from the Black Pine deposit.

Black Pine Montana

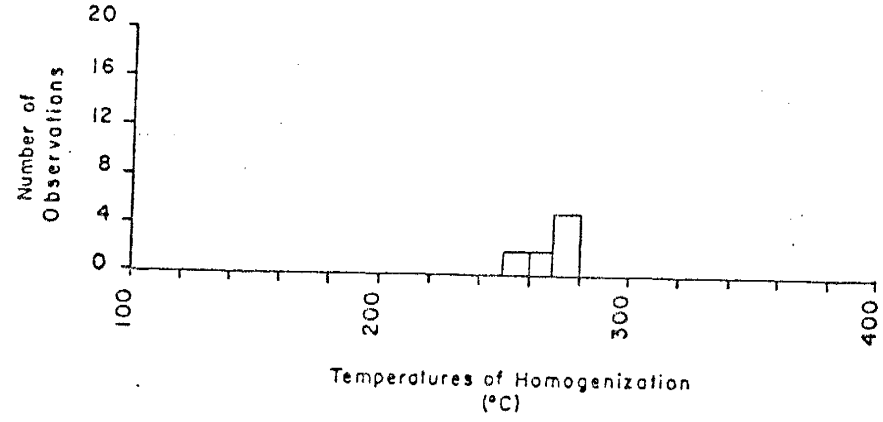

Quartz

A

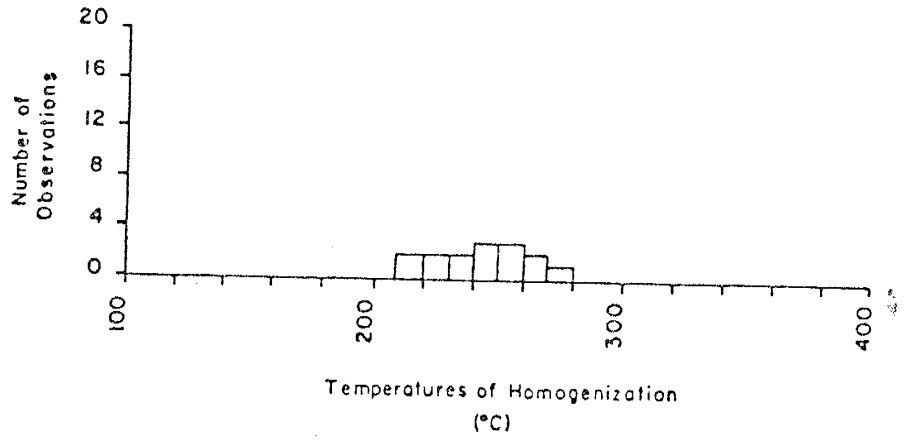

Huebnerite

x=Quartz
o=Wolframite

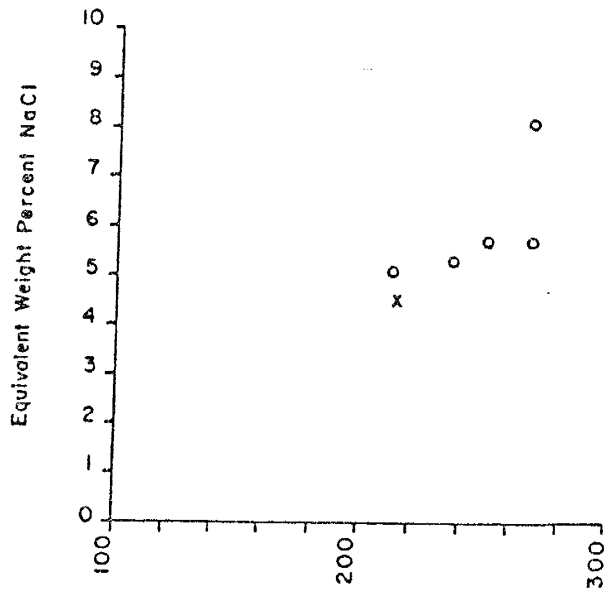

B

INTERPRETATION OF FLUID INCLUSION DATA

Panasqueira, Portugal (PP)

The Panasqueira deposit has been extensively studied by Kelly and Rye (1979). The Panasqueira deposit is an open space filling vein tungsten deposit. Wolframite along with some cassiterite was deposited during the main oxide-silicate stage. The mineral assemblege for this stage includes quartz, muscovite, tourmaline, topaz, arsenopyrite, cassiterite and wolframite. Textures indicate that there was much time overlap and space competition as the open space veins were filled. Wolframite was the earliest ore mineral and appears as isolated crystals and patches in the quartz.

Kelly and Rye (1979) developed a general classification for fluid inclusions from examination of minerals from every stage of mineralization. They developed three general inclusion types.

Type I: Liquid-rich inclusions with >60-70% by volume liquid. The vapor is CO_2 rich (1-2 mole % CO_2). These inclusions homogenized to a liquid. Some contained daughter phases.

Type II: Vapor-rich inclusions with >75% CO_2 rich vapor (14-20 mole % CO_2). These inclusions homogenize to a vapor.

Type III: Liquid-rich inclusions with no vapor phase. These are only found as primary inclusions in the late carbonate stage minerals.

Temperatures of homogenization were determined by Kelly and Rye (1979) from the quartz, topaz and cassiterite of the oxide-silicate stage. It is important to note that the vapor-rich type II inclusions were only found in quartz from this stage. The presence of liquid-rich and vapor-rich inclusions in the same sample indicates boiling or CO_2 effervescence. Thus the temperatures of homogenization are considered to be true temperatures of trapping.

Temperatures determined for the oxide-silicate stage range from 230-360 ^{o}C with a mean at 280^{o}C. Salinities were consistently in the range of 5-10 equivalent weight percent NaCl.

The results of the present study correspond well to Kelly and Rye's data. All three of their general inclusion types were found in wolframite. This is especially notable as the vapor-rich inclusions found in wolframite are only found in quartz from the wolframite stage of mineralization. Temperatures of opacity (170-255^{o}C) can be considered to

represent a minimum above which temperatures of homogenization must occur. This is just below the temperature of homogenization range in the oxide-silicate stage. Salinities collected from wolframite are higher than the range seen in quartz (8-13 equivalent weight percent NaCl for wolframite versus Kelly and Rye's 5-10 equivalent weight percent NaCl in quartz). See figure 19. Not until the late carbonate stage did salinities change, dropping to <5%. It seems unlikely that wolframite formed from a separate fluid when all other evidence indicated a single ore forming fluid.

Figure 19: A plot of salinity measurements from wolframite (this study) and quartz (Kelly and Rye, 1979) from the Panasqueira, Portugal deposit.

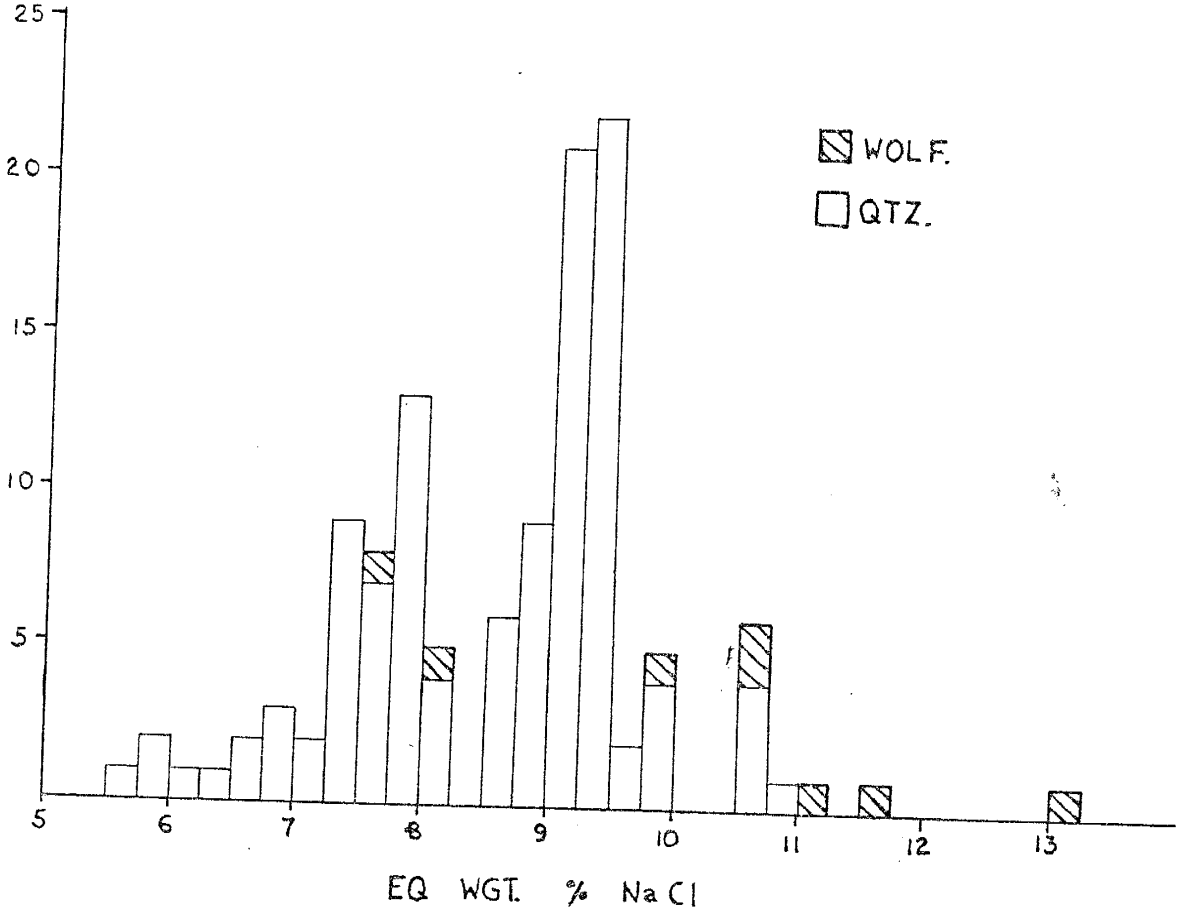
25
20
15
10
5
5
6
7
8
9
10
11
12
13
WOLF.
QTZ.
EQ WGT. % Na Cl

Victorio Mountains, New Mexico (VM)

At this deposit a comparison of the fluid inclusion data obtained from quartz and that obtained from wolframite shows quite a discrepancy. The observable phases in the fluid inclusions at room temperature from each mineral are quite different. These phases provide a rough indication of the fluid compositions. The quartz inclusions are predominantly CO_2-rich. The association of vapor-rich and liquid CO_2-rich inclusions with H_2O-rich inclusions indicates CO_2 effervescence during quartz crystallization. Only one liquid CO_2-rich inclusion was observed in wolframite, the predominant inclusion type being the liquid-rich type I. A comparison of salinities plotted against temperatures of homogenization (figure 16b) shows two distinct populations. The wolframite type I inclusion data plot at higher temperatures (283-378^{o}) and salinities (7.4-8.3) than any of the quartz data. The data from quartz type I CO_2-rich and H_2O-rich inclusions overlap with no indication of separate populations noted. From this graph it is readily apparent that wolframite crystallized from fluids which were significantly different in temperature and composition than those from which quartz crystallized. This relationship is not detectable from observations of hand specimens and thin sections where both minerals seem to be complexly intergrown and cogenetic.

San Cristobal, Peru (SC)

A comprehensive study of the San Cristobal tungsten deposit was done by Campbell (1983) and Campbell et al. (1984). The tungsten stage of mineralization consisted of pyrite, wolframite and quartz with minor augelite and sericite. Fluid inclusions were measured in quartz and augelite by Campbell (1984). The quartz contained two phase inclusions, liquid-rich, which homogenized to a liquid in the range 150-350°C. Of these inclusions, those with a range of temperatures from 150-230°C are considered by Campbell to be secondary inclusions associated with later sphalerite deposition. Those inclusions considered to be primary had a range of temperatures of homgenization of 230-350°C with a mean of 280°C. Salinities in quartz range from 2.7 to 6.3 equivalent weight percent NaCl.

The inclusion data from San Cristobal wolframite measured in this study correlates well with Campbell's data. Temperatures of homogenization in wolframite range from 180-330°C. Using Campbell's primary/secondary cut-off, the mean of wolframite's primary inclusion temperatures of homogenization is 282°C, almost a perfect correlation to the quartz mean of 280°C. The wolframite's salinities also have the same range as that of quartz with 1.6 to 6.6 equivalent weight percent NaCl. A plot of both wolframite and quartz temperatures of homogenization from both studies in figure

20 shows this excellent correlation.

Figure 20: Temperatures of homogenization from wolframite (this study) and quartz (Campbell, 1983).

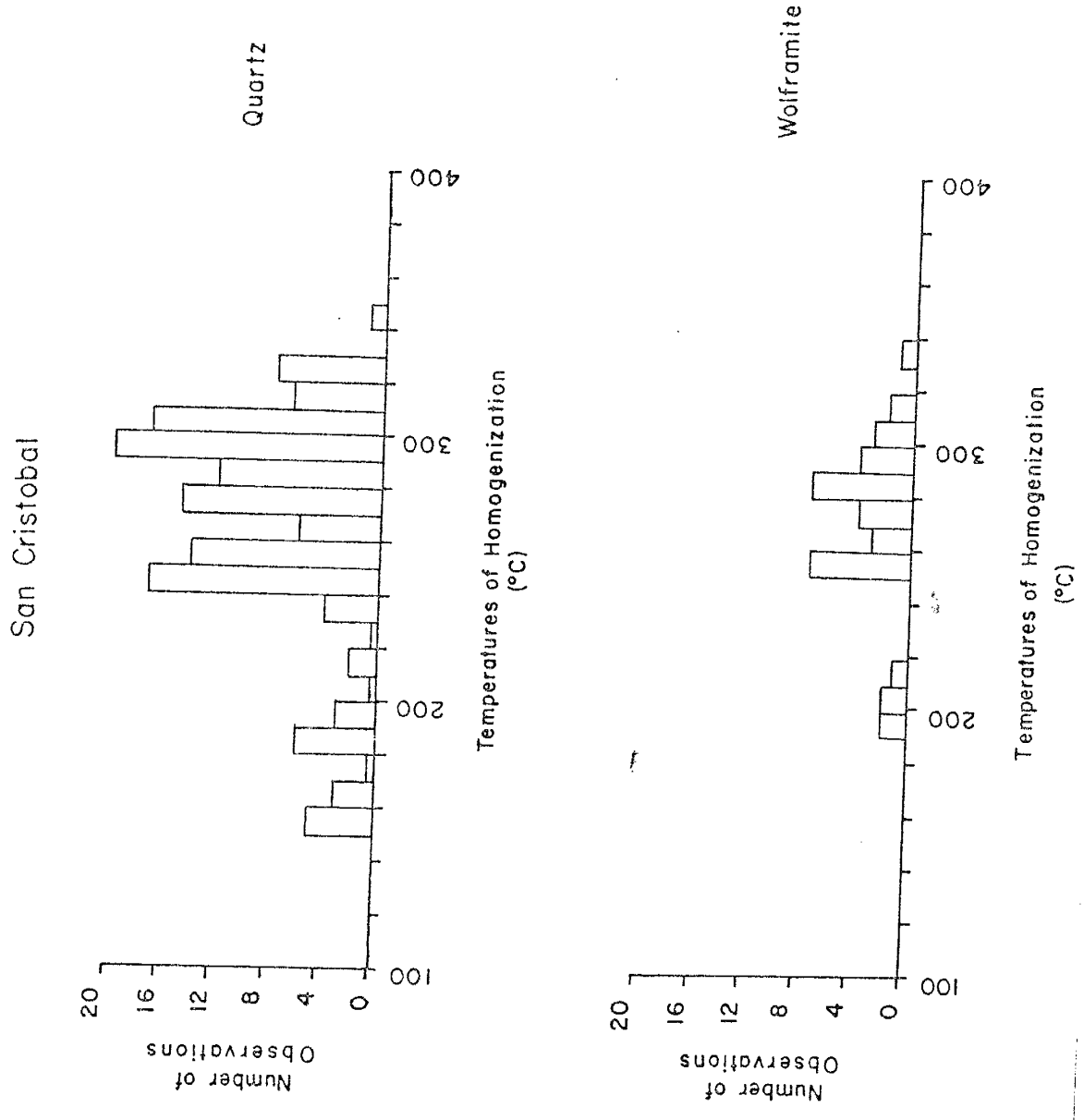
San Cristobal
Quartz
Number of Observations
0
4
8
12
16
20
100
200
300
400
Temperatures of Homogenization (°C)
Wolframite
Number of Observations
0
4
8
12
16
20
100
200
300
400
Temperatures of Homogenization (°C)

Black Pine, Montana (BP)

Black Pine huebnerite exibited a close relationship with quartz, both in fluid inclusion data and in petrographic data. Temperatures of homogenization from both minerals exhibit the same range at 210-280^{o}C. Salinities also agree closely, ranging from 3-6 equivalent weight percent NaCl for huebnerite and 5 equivalent weight percent NaCl for quartz. At this deposit all evidence suggests wolframite and quartz are truely cogenetic.

CONCLUSIONS

The main goal of this aspect of the study was to determine the relationship between wolframite and quartz using microthermometric data. This relationship was then used to analyse the validity of the common assumption that data obtained from transparent gangue is an indication of the conditions existing during ore deposition.

Fluid inclusions were studied and measured in wolframites showing excellent transparency in the infrared. Inclusions in cogenetic quartz were measured and compared to fluid inclusion measurements made in wolframite. To exclude the possibility of changes in fluid inclusion behavior with infrared light, quartz inclusions were examined using infrared and visible light and the data was compared with no significant variation noted.

The relationship between wolframite and quartz for each of the four deposits was studied using standard petrographic observations. Both hand specimens and polished sections gave evidence for a complex intergrown relationship between the two minerals. Such observations are the basis from which a cogenetic relationship is assumed.

Of the four deposits studied, two, San Cristobal and Black Pine, provided identical data from quartz and wolframite. No variation in the measurements of temperatures of homogenization and salinities from each mineral could be determined.

One deposit, Panasqueira, Portugal, indicates a slight difference between the fluid inclusion data obtained from wolframite versus that obtained from quartz as reported by Kelly and Rye (1979). The Panasqueira wolframite had a slightly higher salinity than that obtained from the associated quartz as measured by Kelly and Rye (1979) yet all other observations indicate a strong case for the cogenetic relationship of type I quartz and wolframite at this deposit. It is postulated that the salinity for wolframite may correspond to the higher end of the range reported by Kelly and Rye (1979).

The Victorio Mountains deposit had the most extreme variation between the two data sets. The data indicates that the wolframite was deposited from a high temperature high salinity brine while the quartz was derived from a significantly lower temperature saline, CO_2-rich fluid. Whether this trend is due to an evolving fluid or is an indication of two separate fluids can not be determined. Even so it is quite obvious that the quartz data is hardly sufficient to determine the depositional history of this

deposit.

From this study, the infrared microscope has been proven itself to be of great use in ore deposit research. This instrument has been used to examine fluid inclusions in opaque ore minerals for the first time. This has greatly expanded the amount of data available from the ore deposits studied and allowed for a more complete picture of the process of ore formation.

SUGGESTIONS FOR FUTURE RESEARCH

This study has been a preliminary examination of the uses of the infrared petrographic microscope in ore deposits studies. Several aspects of this study have been only breifly examined in order to limit the scope of the study. There is a need for a futher detailed examination of the geochemistry of wolframite. Using an expanded sample base, the geochemical constituents of wolframite can be analysed to more clearly define a trend of geochemistry with transparency. Infrared spectral studies need to be performed on wolframite to determine the actual wavelengths of infrared light absorbed. A more detailed examination of chemical variations within wolframite banding may answer many questions.

Fluid inclusion studies need to be performed on other minerals in order to further establish the validity of the infrared microscope in ore deposits studies. The list of minerals transparent with this microscope needs to be enlarged. The application of a similar study to the present one in any future fluid inclusion/paragenesis study is obvious. It is hoped that this study is the springboard to a wide range of future uses for the infrared microscope.

APPENDIX I

ANALYTICAL TECHNIQUES

Microprobe

Doubly polished fluid inclusion sections were used as microprobe samples. Microprobe data was collected by Dr. Andrew Campbell at the Los Alamos National Laboratory Microprobe laboratory Los Alamos, New Mexico. Data collected was rough and approximate due to inadequate standards and a data reduction program.

X-ray Fluorescence

The XRF procedures have been previously decribed by Norrish and Chappell (1977) and Jenkins and DeVries (1970). The XRF technique basically involves the comparison of an element's radiation intensity in an unknown sample with that of a standard whose concentration is known.

Sample Preparation

All wolframites were separated from gangue phases (quartz, feldspars and fluorite) by hand picking. This residue was ground by hand with an agate mortar and pestle using acetone as a grinding medium. Further grinding was done using the Microjet-5 high speed grinder with an agate mortar and pestle for 5-10 minutes.

After calculations of mass absorption coefficients for each element, the minimum weight (W) was found to be 0.15 grams.

One to two grams of wolframite powder were pressed with boric acid into a pellet at 20 tons pressure. The pellets were stored in a dry cool room.

Analytical Conditions

The wolframite pellets were analyzed on a Rigaku 3064 X-ray spectrometer. The instrumental parameters are listed below.

INSTRUMENTAL PARAMETERS FOR XRF ANALYSIS

OXIDE	ABSORBER	COUNT TIME (sec)	CRYSTAL	ANGLE (°2θ)	ORDER (n)	COUNTER
SiO2	1	2	RX4	144.52	1	FPC
Al2O3	1	4	PET	144.75	1	FPC
FeO	1	2	LiF 200	57.48	1	SC
MnO	1	2	LiF 200	62.91	1	SC
MgO	1	4	TAP	44.68	1	FPC
CaO	1	8	LiF 220	113.12	1	FPC
Na2O	1	20	TAP	55.10	1	FPC
K2O	1/2	4	LiF 220	136.65	1	FPC
NiO	1	8	LiF 200	48.55	1	SC
CoO	1	40	LiF 200	52.72	1	SC
ZnO	1	10	LiF 200	90.90	2	SC
PbO	1	10	LiF 200	33.82	1	SC
MoO	1	4	LiF 200	20.21	1	SC
Sc2O3	1	40	LiF 200	97.78	1	SC
WO3	1/2	2	LiF 200	42.95	1	SC

Rh tube radiation, 60 Kv 40 Ma

COUNTERS:
SC = scintilation counter
FPC = flow proportional counter
ABSORBER = intensity attenuator
CRYSTAL = analysing diffracting crystal
PET = Penta Erythratol
TAP = Thalium Acid Pthalale
LiF = Lithium Fluoride d=(200) or (220)
ORDER n = Order of the counted reflection

Counts were made using a fixed time optimum set up. Data were collected and converted into intensities and concentrations by comparison with calibration curves developed with two wolframite standards and three silicate

standards. The accepted chemical analyses of the standards are listed below. The calibrations were done using the fundamental parameters program, XRF-11, a product of Criss Software, Inc. Largo, Maryland, on a DEC PDP 11/23. This program calculates theoretical XRF intensities and alpha coefficients from fundamental parameters. The program SCRAP corrected for dead time losses, background, tube line interference, line overlap from other elements and made mass absorption corrections.

COMPOSITIONS OF STANDARDS IN WEIGHT PERCENT

	FeWO4	MnWO4	Sy-3,9	NIM-D	VS-N
SiO	---	---	59.68	38.96	56
Al2O3	---	---	11.80	0.3	13.5
FeOt	23.7	---	5.78	15.34	4.1
MnO	---	23.4	0.32	0.22	0.11
MgO	---	---	2.67	43.51	4.5
CaO	---	---	8.26	0.28	4.6
Na2O	---	---	4.15	0.04	6.0
K2O	---	---	4.2	0.01	8.1
NiO	---	---	---	0.25	0.08
CoO	---	---	---	---	0.09
ZnO	---	---	---	---	0.08
PbO	---	---	---	---	0.11
MoO3	---	---	---	---	0.11
Sc2O3	---	---	---	---	0.046
WO3	76.3	76.6	---	---	---

Minimum relative error in the XRF measurments were calculated using the count rate for each element [R_p] and the count rate for each element's background [R_b] as is shown in the following equation:

$$\text{ERROR} = (\sqrt{R_p + R_b}) \; / \; (R_p - R_b)$$

These errors are listed as (+/-) percents in the following table:

MINIMUM RELATIVE ERROR FOR XRF ANALYSIS

OXIDE	BP	PP	VM	NV	MO	BN	SD	CE	TT	HK	SP	JP	WO
WO3	0.5	0.5	0.5	0.5	0.5	0.5	0.5	0.5	2	0.5	0.5	0.5	0.5
FeO	13.6	0.5	0.9	2	1	0.6	0.7	0.6	0.6	0.7	0.7	0.6	7.5
MnO	0.6	1.4	0.6	0.6	0.8	1.4	0.8	1	2	0.8	0.8	1	0.6
SiO2	5	5	3	2	3	3	0.6	1	4	1	0.7	2	2
Al2O3	---	13	5	33	9	17	45	26	9	2	3	6	27
MgO	---	83	64	---	---	53	---	---	15	---	---	64	---
CaO	20	17	2	29	---	2	2	9	5	2	---	10	4
Na2O	89	---	519	---	---	---	---	488	---	873	---	526	254
K2O	64	15	24	43	21	41	83	36	19	3	5	25	50
Sc2O3	---	---	67	---	---	---	34	---	---	---	---	73	---
CoO	---	---	120	---	---	---	---	---	---	---	---	114	---
NiO	18	18	16	19	19	15	21	19	19	19	18	20	20
ZnO	24	37	16	34	39	52	49	49	14	56	68	45	62
PbO	---	29	4	11	1	---	39	---	9	45	8	86	---
MoO3	118	132	23	---	---	---	188	122	---	98	---	151	---

X-ray Diffraction

Sample Preparation

The pressed powder boric acid pellets made for XRFS were used for the samples of each wolframite sample. (See sample preparation, XRFS).

All runs were made on a Rigaku x-ray diffractometer equipped with a monochromator using CuKa radiation at 40Kv and 25Ma and a scintillation counter. Individual XRD runs were made of each sample using a step scan of 0.020° 2θ at 0.20 second count time. The scan was performed over the range from 13 to 70° 2θ.

Neutron Activation Analysis

Ten samples were selected to be irradiated at the Sandia Laboratory Reactor in Albuquerque, New Mexico. These samples were selected so that the full range of transparency observed in wolframite was represented. Samples for neutron activation analysis were prepared and analysed by Dr. Phillip Kyle of NMIMT.

APPENDIX II

FLUID INCLUSION DATA

PANASQUEIRA, PORTUGAL

MINERAL	SAMPLE NUMBER	TYPE	Th (°C)	Tm (°C)	eq. wgt. % NaCl
wolframite	WP0	II	201	-7.5	11.1
wolframite	WP0	II	204	-7.2	10.9
wolframite	WP0	II	216	-6.5	9.9
wolframite	WP0	II	180	---	---
wolframite	WP0	II	---	-0.2	0.35
wolframite	PGL-303	II	---	-7.8	11.5
wolframite	PGL-303	II	---	-9.3	13.2
wolframite	PGL-279	II	---	-7.0	10.5
wolframite	PGL-279	II	253	---	---
wolframite	PGL-279	II	253	---	---
wolframite	PGL-303	II	---	-4.8	7.6
wolframite	PGL-303	II	---	-5.1	8.0
wolframite	PGL-303	II	---	-10.9	14.9
MEAN			218		10.8

VICTORIO MOUNTAINS, NEW MEXICO

MINERAL	SAMPLE NUMBER	TYPE	Th (°C)	Tm (°C)	eq. wgt. % NaCl
wolframite	V-1	I	359	---	---
wolframite	V-1	I	359	---	---
wolframite	V-6	I	355	---	---
wolframite	V-6	I	355	---	---
wolframite	V-6	I	352	---	---
wolframite	V-6	I	353	---	---
wolframite	V-6	I	326	---	---
wolframite	V-6	I	359	---	---
wolframite	V-6	I	353	-4.5	7.5
wolframite	V-6	I	359	-5.8	8.4
wolframite	V-6	I	352	---	---
wolframite	V-6	I	345	---	---
wolframite	V-6	I	336	---	---
wolframite	V-6	I	283	---	---
wolframite	V-6	I	310	---	---
wolframite	V-6	I	336	---	---
wolframite	V-6	I	322	---	---
wolframite	V-7	I	338	---	---
wolframite	V-7	I	336	-3.3	5.4
wolframite	V-7	I	341	-4.8	7.6
wolframite	V-7	I	311	---	---
wolframite	V-7	I	378	---	---
wolframite	V-7	I	356	-5.3	8.3
wolframite	V-7	I	342	-4.7	7.4
wolframite	V-7	I	362	-4.9	7.7
wolframite	V-7	I	366	---	---
wolframite	V-7	I	337	-4.7	7.4
wolframite	V-7	I	363	---	---
MEAN			344		7.5
quartz	V-14	I	195	---	---
quartz	V-14	I	177	---	---
quartz	V-14	I	168	---	---
quartz	V-14	I	141	---	---
quartz	V-14	I	173	---	---
quartz	V-14	I	192	---	---
quartz	V-14	I	163	---	---
quartz	V-14	I	176	---	---
quartz	V-14	I	188	---	---
quartz	V-14	I	248	---	---
quartz	V-14	I	240	---	---
quartz	V-14	I	246	---	---
quartz	V-14	I	236	---	---
quartz	V-14	I	242	---	---
quartz	V-14	I	262	-8.2	11.9
quartz	V-14	I	306	-3.0	4.9
quartz	V-14	I	239	-6.0	9.2

quartz	V-14	I	258	-6.3	9.6
quartz	V-14	I	262	-2.1	3.5
quartz	V-14	I	313	-1.9	3.2
quartz	V-14	I	199	---	---
quartz	V-14	I	290	---	---
quartz	V-14	I	202	-4.8	7.6
quartz	V-14	I	200	-4.0	6.4
quartz	V-14	I	185	-4.2	6.7
quartz	V-14	I	191	-1.0	1.7
quartz	V-14	I	198	-1.5	2.6
quartz	V-14	I	179	-0.4	0.7
quartz	V-14	I	172	-0.2	0.35
quartz	V-14	I	208	---	---
quartz	V-14	I	187	---	---
quartz	V-14	I	256	---	---
quartz	V-14	I	236	---	---
quartz	V-3	I	164	-0.8	1.4
quartz	V-3	I	177	-1.1	1.9
quartz	V-14	II	262	8.0	4.0
quartz	V-14	II	254	4.4	10.0
quartz	V-14	II	300	4.5	9.8
quartz	V-14	II	231	4.9	9.5
quartz	V-14	II	317	7.5	5.8
quartz	V-14	II	210	-0.9	16.8
quartz	V-14	II	244	8.0	4.0
quartz	V-14	II	260	8.5	3.0
quartz	V-14	II	295	9.4	1.5
quartz	V-14	II	261	9.4	1.5
quartz	V-14	II	268	9.6	1.3
quartz	V-14	gas-II	261	---	---
MEAN			203		

SAN CRISTOBAL, PERU

MINERAL	SAMPLE NUMBER	TYPE	Th (°C)	Tm (°C)	eq. wgt. % NaCl
wolframite	SC-8025	I	251	---	---
wolframite	SC-8025	I	251	---	---
wolframite	SC-8025	I	317	---	---
wolframite	SC-8025	I	208	---	---
wolframite	SC-8025	I	199	---	---
wolframite	SC-2	I	256	---	---
wolframite	SC-7	I	195	---	---
wolframite	SC-7	I	252	---	---
wolframite	SC-9	I	264	---	---
wolframite	SC-9	I	283	---	---
wolframite	SC-9	I	268	---	---
wolframite	SC-9	I	270	---	---
wolframite	SC-9	I	207	---	---
wolframite	SC-9	I	219	---	---
wolframite	SC-9	I	270	---	---
wolframite	SC-9	I	256	-0.9	1.6
wolframite	SC-9	I	272	-3.9	6.3
wolframite	SC-9	I	289	-3.5	5.7
wolframite	SC-9	I	310	---	---
wolframite	SC-9	I	283	---	---
wolframite	SC-9	I	302	-1.0	1.7
wolframite	SC-9	I	285	-3.3	5.4
wolframite	SC-9	I	288	---	---
wolframite	SC-9	I	330	---	---
wolframite	SC-9	I	258	-4.1	6.6
wolframite	SC-9	I	253	---	---
wolframite	SC-9	I	286	-3.0	4.9
wolframite	SC-9	I	292	---	---
wolframite	SC-9	I	285	---	---
wolframite	SC-9	I	296	---	---
wolframite	SC-9	I	263	-2.4	4.0
wolframite	SC-9	I	300	-3.3	5.4
wolframite	SC-9	I	300	-2.7	4.5
wolframite	SC-9	I	293	-3.0	4.9
wolframite	SC-9	I	271	---	---
wolframite	SC-9	I	293	---	---
wolframite	SC-9	I	---	-3.5	5.7
MEAN			270		4.7
quartz	SC-8045	I	227	---	---
quartz	SC-8045	I	200	---	---
quartz	SC-2	I	240	---	---
quartz	SC-2	I	267	---	---
quartz	SC-2	I	274	---	---
quartz	SC-2	I	220	---	---
quartz	SC-2	I	264	---	---

quartz	SC-2	I	150	---	---
quartz	SC-2	I	245	---	---
quartz	SC-2	I	246	---	---
quartz	SC-2	I	240	---	---
quartz	SC-2	I	256	---	---
MEAN			236		---

BLACK PINE, PHILLIPSBURG, MONTANA

MINERAL	SAMPLE NUMBER	TYPE	Th (°C)	Tm (°C)	eq. wgt. % NaCl
huebnerite	BP-1	I	234	---	---
huebnerite	BP-1	I	225	---	---
huebnerite	BP-1	I	246	---	---
huebnerite	BP-1	I	227	---	---
huebnerite	BP-1	I	215	---	---
huebnerite	BP-1	I	257	---	---
huebnerite	BP-1	I	274	---	---
huebnerite	BP-1	I	260	---	---
huebnerite	BP-1	I	250	---	---
huebnerite	BP-1	I	260	---	---
huebnerite	BP-1	I	247	---	---
huebnerite	BP-1	I	257	---	---
huebnerite	BP-1	I	247	---	---
huebnerite	BP-1	I	212	---	---
huebnerite	BP-1	I	---	-5.2	8.1
huebnerite	BP-1	I	---	-4.8	7.6
huebnerite	BP-1	I	---	-3.5	5.7
huebnerite	BP-1	I	---	-3.5	5.7
huebnerite	BP-1	I	---	-3.3	5.3
huebnerite	BP-1	I	---	-3.1	5.1
MEAN			244		6.25
quartz	BP-1	I	270	---	---
quartz	BP-1	I	264	---	---
quartz	BP-1	I	264	---	---
quartz	BP-1	I	274	---	---
quartz	BP-1	I	252	---	---
quartz	BP-1	I	270	---	---
quartz	BP-1	I	272	---	---
quartz	BP-1	I	254	---	---
quartz	BP-1	I	---	-2.7	4.5
quartz	BP-1	I	272	---	---
MEAN			266		

BIBLIOGRAPHY

Bailly, R., 1938, Emploi de l'infra-rouge dans l'etude des mineraux opaques: Acad. Royale Belgique Bull., Cl. Sci., no. 12, p. 791-822.

Bailly, R., 1942, Proprietes optiques du wolfram: Ann. Soc. Geol. Belgique, vol. 65 Bull. p. B133-B139. (Min. Abs.)

Baumann, L. and Starke, R., 1965, Beitrag zur Verteilung der H/F Koeffizienten innerhalb der Wolframitlagerstatte Pechtelgrun auf Grund neuer rontgenographischer Untersuchungen: Bergakademie, vol. 16, p. 79-82.

Berman, J. and Campbell, W., 1957, Relationship of composition to thermal stability in the huebnerite-ferberite series of tungstates: U.S. Bur. Mines Rep. Invest. 5300, 14p.

Berzina, I.B. and Dolomanova, E.I., 1967, Uranium content in cassiterites, determined from traces of fragments caused by uranium fission: Doklasy, Earth Science Section, Vol. 175, p. 114-118.

Burns, R.G., 1970, Mineralogical applications of crystal field theory: Cambridge, Cambridge Univ. Press, 224 p.

Campbell, A.R., 1983, Genesis of the tungsten-base metal ores at San Cristobal, Peru: Unpub. Ph.D. thesis, Harvard Univ., 176 p.

Campbell, A.R., Rye, D., Petersen, U., 1984, A Hydrogen and Oxygen Isotope Study of the San Cristobal Mine, Peru: Implications of the Role of Water to Rock Ratio for the Genesis of Wolframite Deposits: Econ. Geol. vol. 79 p. 1818-1832.

Campbell, A.R., Hackbarth, C.J., Plumlee, G.S., and Petersen, U., 1984, Internal Features of Ore Minerals Seen with the Infrared Microscope: Econ. Geol. vol. 79 p. 1387-1392.

Carmichael, R.S., 1985, CRC Handbook of Physical Properties of Rocks: Vol. I: Mineral Composition, CRC Press, 416 p.

Collins, P.F., 1979, Gas hydrates in CO2-bearing fluid inclusions and the use of freezing data for estimation of salinity: Econ. Geol. vol. 74 p. 1435-1444.

Cuff, C., 1979, In Geology of tin deposits: R. G. Taylor (ed.) Elsevier.

Cullity, B.D., 1956, Elements of X-ray Diffraction: Reading, Mass., Addison-Wesley Publ., 514 p.

Emmons, S.F., Eckel, E.C., 1905, Contributions to Economic Geology, Copper Mines of the United States: U.S.G.S. Bull. 285, p. 99-103.

Emmons, S.F., 1907, Contributions to Economic Geology, Gold Silver Deposits: U.S.G.S. Bull. 315, p. 36-45

Ganeev, I.G. and Sechina, N.P., 1960, The Geochemical Peculiarities of wolframite: Geochemistry 6, p. 617-623.

Goncharov, G.N. and Filatov, S.K., 1971, The typical structural features of cassterite from Sherlovaya Gora: Geochemistry International, Vol. 8, p. 268-275.

Gorgees, C., 1974, Geology and mineralisation at Herberton Hill, Herberton, North queensland, Australia: Unpubl. Thesis, James Cook Univ. of N. Queensland, Australia.

Griswold, G.B., 1959, Mineral Deposits of Lincoln County, New Mexico: NMBMMR Bull. 67, 157 p.

Guillen, R. and Regnard, J.R., 1985, Magnetic Properties of Natural and Synthetic Wolframites $Fe_xMn_{1-x}WO4$: Phys Chem Minerals, vol. 12, p. 246-254.

Hayes, C.W. and Lindgren, W., 1908, Contributions to Economic Geology, Part I-Metals and Nonmetals, Except Fuels: U.S.G.S. Bull. 380, p. 131-163.

Hess, F.L., 1909, Note on a Wolframite Deposit in the Whetstone Mountains, Arizona: U.S.G.S. Bull. 390, p. 164-165.

Hess, F.L., 1917, Tungsten Minerals and Deposits: U.S.G.S. Bull. 652.

Holland, R.A.G., Bray, C.J. and Spooner, E.T.C., 1978, A method for preparing doubly polished thin sections suitable for microthermometric examination of fluid inclusions: Mineral. Mag., vol. 42 p. 407-408.

Jenkins, R. and De Vries, J.L., 1970, Practical X-Ray Spectrometry: 2nd Edition, Springer-Verlag New York, Inc.

Kelly, W.C. and Turneaure, F.S., 1970, Mineralogy, Paragenesis and Geothermometry of the Tin and Tungsten Deposits of the Eastern Andes, Bolivia: Econ. Geol. Vol. 65, p. 609-680.

Kelly, W.C. and Rye, R.O., 1979, Geologic, Fluid Inclusion, and Stable Isotope Studies of the Tin-Tungsten Deposits of Panasqueira, Protugal: Econ. Geol. vol. 74, p. 1721-1818.

Landis, G.P and Rye, R.O.,1974, Geologic, Fluid Inclusion, and Stable Isotope Studies of the Pasto Buena Tungsten-Base Metal Ore Deposit, Northern Peru: Econ. Geol. vol. 69 p. 1025-1059.

Moore, F. and Moore, D.J., 1979, Fluid-inclusion study of mineralization at St. Michael's Mount, Cornwall: Trans. Inst. Mining Metall. B, vol. 88, p. 57-60.

Noll, W., 1949, Crystal chemistry of cassiterite: Heidelberger. Beitrage zur Mineralogie und Petrographie. vol. 1, p. 593-625. (English Abstract: Chemical Abstracts, 1950, vol. 44, p. 490i).

Norrish, K. and Chappell, B.W., 1977, in Physical Methods in Determinative Mineralogy: 2nd Edition. Edited by J Zussman, Academic Press New York, Chapter 5 p. 201-272.

Northrup, S.A., 1959, Minerals of New Mexico: Univ. of New Mexico Press, p. 557-558.

Palache, C., Berman, H., and Frondel, C., 1951, Dana's System of Mineralogy, 7th Ed., Vol. 2: New York, Wiley and Sons, Inc., 1124 p.

Pecora, W.T., Switzer, G., Barbosa, A.L., and Myers, A.Y., 1950, Structure and mineralogy of the Golconda pegmatite, Minas Gerais, Brazil: American Mineralogist, vol. 35 p. 889-901.

Potter, II, R.W., Clynne, M.A., and Brown, D.L., 1978, Freezing point depression of aqueous sodium chloride solutions: Econ. Geol., vol. 73 p. 284-285.

Roedder, E., 1984, Reviews in Mineralogy vol. 12, Fluid Inclusions: Mineralogical Society of America, 644 p.

Saldanha, R., 1947, O estudo da jazida de wolframita de Inhandjara: Mineralogical Abstracts v. 10, p. 230.

Sasaki, A., 1959, Variation of unit cell parameters in wolframite series: Miner Journal, vol. 2 p. 375-396.

Sawkins, F.J., 1966, Preliminary fluid inclusion studies of the mineralization associated with the Hercynian granites of Southwest England: Inst. Mining Met. Trans. vol. 75 p. B109-B112.

Sleight, A.W., 1972, Accurate cell dimensions for ABO_4 Molybdates and Tungstates: Acta Crystallogr. B28, p. 2899-2902.

Swart, P.K. and Moore, F., 1982, The occurrence of uranium in association with cassiterite, wolframite, and sulphide mineralization in South-West England: Mineralogical Magazine, vol. 46 p. 211-215.

Taylor, R.G., and Hosking, K.F.G., 1970, Manganese-Iron Ratios in Wolframite, South Crofty Mine, Cornwall: Econ. Geol. vol. 65 p. 47-53.

Thorman, C.H., and Drewes, H. 1978, Geology of the Gary and Lordsburg quadrangles, Hidalgo County, New Mexico: U.S. Geol. Survey Misc. Geol. Invest. Map I-1151.

Tolman, C., 1933, The Geology of the Silver Mine Area, Madison County Missouri: Reprint of Appendix I, 57th Biennial Report Missouri Bureau of Geology and Mines.

Ulku, D., 1967, Untersuchemgen zur Kristallstruktur und magnetischen Struktur des Ferberits FeWO4: Zeit. fur Kristall. Bd., Vol.124, p. 192-219.

Volin, M.E., Roby, R.N., and Cole, J.W., Investigation of the Combination Silver-Tungsten Mine, Granite county, Montana: U.S. Bureau of Mines Report of Investigations no. 4914.

Weast, R.C. (editor), 1978, CRC Handbook of Chemictry and Physics, 59th Edition, CRC Press, Boca Raton, Florida, p. F-253.

Weeks, F.B., 1908, Tungsten Deposits in the Snake Range, White Pine County, Eastern Nevada: U.S.G.S. Bull. 340, p. 263-270.

This thesis is accepted on behalf of the faculty of the Institute by the following committee:

Andrew Campbell
Advisor

Frederick J. Kuehnast

April 25 1986
Date